

New Results on Absorbing Layers and Radiation Boundary Conditions

Thomas Hagstrom*

Department of Mathematics and Statistics
The University of New Mexico
Albuquerque, NM 87131

and

Institute for Computational Mechanics in Propulsion
Ohio Aerospace Institute and NASA Glenn Research Center
Cleveland, OH 44142
hagstrom@math.unm.edu

1 Introduction

Perhaps the defining feature of waves is the fact that they propagate long distances relative to their characteristic dimension, the wavelength. This allows us to use them to probe the world around us - optically, acoustically, and now at a wide range of wavelengths in a variety of media. For numerical simulations, it is precisely this essential characteristic - the radiation of waves to the far field - that leads to the greatest difficulties. One may view this fundamental difficulty as rooted in the existence of (at least) two widely separated spatial scales. The first are the small scales associated with the wavelengths and the scatterer, and the second is the long distance between the scatterer and the observers.

The techniques discussed in this review are designed to make the accurate and efficient solution of typical wave propagation problems possible by restricting the computation to the small scale only. We do this, of course, by introducing an artificial boundary, Γ , and either imposing absorbing boundary conditions on it or surrounding it with an absorbing layer. Typical configurations are shown in Figure 1 below.

Our focus here will be on time-domain problems for the standard equations of wave theory - the scalar wave equation, first order hyperbolic systems, and the Schrödinger equation. Although frequency-domain calculations still dominate much applied work, we believe that time-domain simulations will become increasingly important to efficiently study broadband problems and nonlinear scatterers and sources. Moreover, in the frequency domain accurate boundary conditions and integral equation methods are well-established, and

* Supported in part by NSF Grant DMS-9971772 and NASA Contract NAG3-2692. Any opinions, findings, and conclusions or recommendations expressed in this paper are those of the author and do not necessarily reflect the views of NSF or NASA.

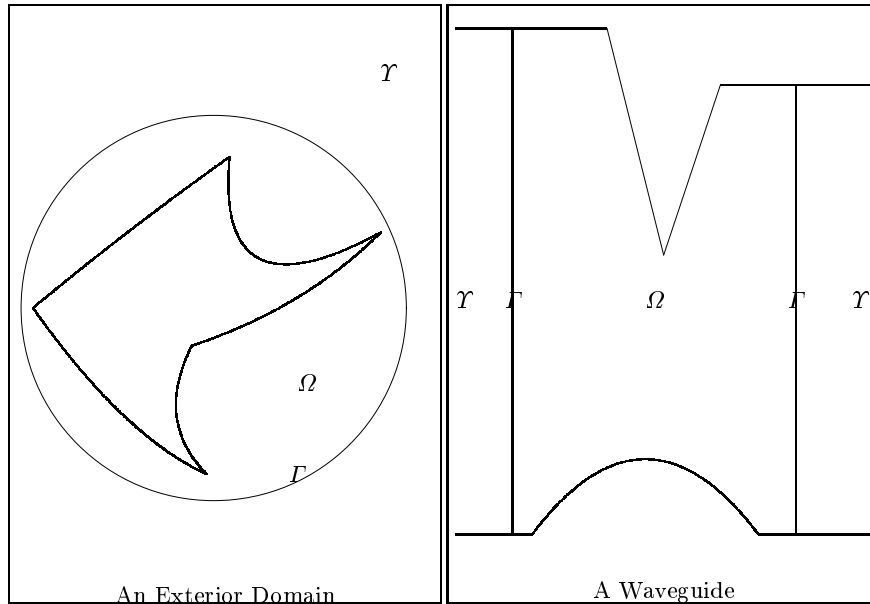


Fig. 1. Typical domain configurations. Ω is the computational domain, Γ is the artificial boundary, Υ is the tail.

the costs associated with them are fundamentally easier to control. (See, e.g. [33, 38, 85].)

In 1999, the author wrote a lengthy review of the state-of-the-art in radiation boundary conditions for time-dependent problems [47]. Even then it was clear that for many important problems a number of satisfactory methods were available. Since then, new developments have provided the practitioner with a wider range of tools and raise the hope of solving the still-open problems listed in [47]. Within the narrower scope of the current work, we will review that state-of-the-art along with later contributions. Our primary goal is to explain in detail the methods that work and to illustrate their performance. We will also revisit some unsolved cases and speculate on their potential resolution.

Prior to the early nineties, the usual approach to truncating the domain was to fix some low order absorbing boundary condition. If the accuracy provided was insufficient, improvements could be made by increasing the domain size. The latter approach is both inconvenient to carry out automatically and, for three-dimensional problems in particular, rather expensive. Thus, in practice, there was no way to achieve convergence to a prescribed tolerance. The fundamental breakthroughs which changed the situation were:

- i. The realization that the boundary condition hierarchies proposed a decade earlier [78, 26, 27, 16, 61, 60] could, in fact, be stably and conveniently implemented using auxiliary functions defined only on the boundary [18, 49, 35]¹;
- ii. Proofs and/or numerical demonstrations of the rapid convergence with increasing order of the solutions produced by these hierarchies [45, 46, 49, 104];
- iii. Low storage and fast methods to directly impose nonlocal conditions [89, 40, 41, 5, 6, 28, 86, 80];
- iv. Parallel development of the perfectly matched layer (PML), an absorbing layer with a reflectionless interface [14, 17, 94, 20, 96, 82].

As mentioned earlier, the new methods provide, in many circumstances, a satisfactory solution to our problem. That is, first, they enable us to meet any prescribed error tolerance at a cost no greater than the cost of solving the interior problem. And, second, they allow us to compute on a domain which scales with the size of the scatterer, independent of solution time or error tolerance. Our hope in this paper is to explain how and why they work, focusing on the case we understand best: the scalar wave equation and its relatives.

We will illustrate many of the techniques with numerical experiments. Often these were executed with the author's research codes. The latter can be downloaded from www.math.unm.edu/~hagstrom/downloads. The reader is cautioned, however, that these are research codes which are not consistently documented, and that they come with no warranty whatsoever. I would also like to acknowledge the collaboration of a number of others in the work described below: Dr. Brad Alpert of NIST-Boulder, Dr. John Goodrich of NASA Glenn, Prof. Leslie Greengard of the Courant Institute, Prof. S.I. Hariharan of the University of Akron, Prof. Tim Warburton of UNM, Dr. Liyang Xu of MZA, and Igor Nazarov, currently a doctoral student at UNM.

2 Boundary Conditions

To develop useful approximate boundary conditions, it is fruitful to consider first the construction of exact boundary conditions. Plainly speaking, the condition we wish to impose is that the solution and any necessary derivatives at the boundary be the trace of an element of the set of outgoing solutions - precisely solutions of the homogeneous problem in \mathcal{Y} which are initially zero. One can generally derive concrete expressions for the boundary condition by performing a Laplace transformation in time with dual variable s . Taking $\Re s$ sufficiently large, the transformed problem typically has an exponential dichotomy. The exact boundary condition is then given by an appropriate

¹ Lindman, in the earliest of these works [78], actually suggests the auxiliary variable method.

projection of the solution onto the exponentially decaying subspace. Although this cookbook construction may seem difficult, we see that sometimes we can carry it through.

2.1 The Wave Equation with a Cylindrical Tail

We begin with the simplest case, namely when the equation in the tail, \mathcal{Y} , is the scalar wave equation. Suppose we are in the first case shown in Figure 1, so that \mathcal{Y} is the cylinder $(x, y) \in (0, \infty) \times \Xi$. We suppose the equation in the tail is given by:

$$\frac{1}{c^2} \frac{\partial^2 u}{\partial t^2} = \frac{\partial^2 u}{\partial x^2} + L(y, \partial/\partial y)u, \quad (1)$$

with some homogeneous boundary conditions on $\partial\Xi$. We explicitly assume that u is initially zero in \mathcal{Y} . We suppose L in concert with the boundary conditions is some negative, self-adjoint, linear elliptic operator with associated eigenvalues-eigenvectors:

$$L\psi_j = -\kappa_j^2\psi_j, \quad j = 1, \dots, \infty, \quad (2)$$

$$\int_{\Xi} \psi_j^2 dy = 1. \quad (3)$$

Expanding u in a Fourier series in the ψ_j and performing a Laplace transform in t we obtain the equation:

$$\frac{\partial^2 \hat{u}_j}{\partial x^2} = \left(\frac{s^2}{c^2} + \kappa_j^2 \right) \hat{u}_j, \quad x > 0. \quad (4)$$

Clearly, the causal solution must vanish for x large and t small. Choosing $\Re s > 0$ we see that (4) has only one bounded solution, which must solve the original problem:

$$\hat{u}_j(x, s) = e^{-(c^{-2}s^2 + \kappa_j^2)^{1/2}x} \hat{u}_j(0, s), \quad (5)$$

where the branch is chosen so that:

$$\Re(c^{-2}s^2 + \kappa_j^2)^{1/2} > 0, \quad \Re s > 0. \quad (6)$$

This implies the following exact boundary condition at $x = 0$, which we write in two forms:

$$\frac{\partial \hat{u}_j}{\partial x} + c^{-1}s\hat{u}_j + \frac{\kappa_j^2}{c^{-1}s + (c^{-2}s^2 + \kappa_j^2)^{1/2}}\hat{u}_j = 0, \quad (7)$$

$$(c^{-2}s^2 + \kappa_j^2)^{-1/2} \frac{\partial \hat{u}_j}{\partial x} + \hat{u}_j = 0. \quad (8)$$

Inverting these we obtain, respectively:

$$\frac{\partial u}{\partial x} + \frac{1}{c} \frac{\partial u}{\partial t} + \mathcal{F}^{-1} (K_j(t) * (\mathcal{F}u(0, \cdot, \cdot))) = 0, \quad (9)$$

$$\mathcal{F}^{-1} \left(W_j(t) * \left(\mathcal{F} \frac{\partial u}{\partial x}(0, \cdot, \cdot) \right) \right) + u = 0. \quad (10)$$

(The first form is the one we have typically used, while the second has been used in [80].) Here, \mathcal{F} is the Fourier series with respect to the eigenfunctions of L . The convolution kernels, K_j and W_j , can, in fact, be explicitly represented in terms of Bessel functions, but in general we work with their transforms directly.

Both (9) and (10) are nonlocal in space and time. However, this nonlocal operator factors into the composition of purely spatial and purely temporal operators. In many cases, for example when $L = \nabla^2$, \mathcal{F} and \mathcal{F}^{-1} can be applied using the FFT. Also, the temporal convolution can be treated by the algorithm in [54]. Then the cost of applying the exact nonlocal condition is acceptable. However, these algorithms require full history storage at the boundary, which is prohibitive except when the solution times are relatively short. We remark (see also [80]) that the kernels do define standard Volterra integral operators. In contrast, the retarded potential operator arising in direct integral equation formulations of the wave equation is nonstandard. The improved operators are a direct consequence of using the Dirichlet-to-Neumann or Neumann-to-Dirichlet maps.

The primary difficulty, then, is to remove the temporal and, possibly, the spatial nonlocality. The main observation is that convolution with exponential functions can be performed without storing the history, but instead by solving a differential equation. If

$$\phi(t) = \int_0^t \alpha e^{-\beta(t-z)} v(z) dz, \quad (11)$$

then

$$\frac{d\phi}{dt} + \beta\phi = \alpha v, \quad \phi(0) = 0. \quad (12)$$

For the transformed variables we have:

$$\hat{\phi}(s) = \frac{\alpha}{s + \beta} \hat{v}. \quad (13)$$

The idea, then, is to construct convergent sequences of exponential approximations, $A_j^{q_j}$, to the kernels, K_j in (9) or W_j in (10), at least on finite time intervals. Working in transform space, this is equivalent to constructing rational approximations to their transforms in right half planes. To make this precise we recall the simple estimate based on Parseval's relation:

$$\|(K_j - A_j^{q_j}) * v\|_{L_2(0,T)} \leq C e^{\eta t} \sup_{\Re s \geq \eta} |\hat{K}_j(s) - \hat{A}_j^{q_j}(s)| \cdot \|v\|_{L_2(0,T)}. \quad (14)$$

We construct $\hat{A}_j^{q_j}$ to be a rational function of degree $(q_j - 1, q_j)$. It then admits a partial fraction decomposition:

$$\hat{A}_j^{q_j} = \sum_{k=1}^{q_j} \frac{\alpha_{jk}}{s + \beta_{jk}}, \quad (15)$$

and

$$A_j^{q_j} * v = \sum_{k=1}^{q_j} \phi_{jk}(t), \quad (16)$$

$$\frac{d\phi_{jk}}{dt} + \beta_{jk}\phi_{jk} = \alpha_{jk}v, \quad \phi_{jk}(0) = 0. \quad (17)$$

Thus we have approximated the temporal convolution by a system of differential equations for auxiliary functions defined on the boundary only. The work per time step and storage required is proportional to the number of eigenfunctions, ψ_j , the number of auxiliary functions, q_j , and the cost of computing and inverting the Fourier series.

We note that the boundary condition is also localizable in space if the j -dependence of the rational approximations can be described by polynomials in the eigenvalues, κ_j^2 . We then have:

$$\hat{A}_j^{q_j} = \frac{N(s, \kappa_j^2)}{D(s, \kappa_j^2)}. \quad (18)$$

Formally (9) becomes:

$$\frac{\partial u}{\partial x} + \frac{\partial u}{\partial t} + w = 0, \quad (19)$$

$$D\left(\frac{\partial}{\partial t}, L\right)w = N\left(\frac{\partial}{\partial t}, L\right)u. \quad (20)$$

Of course we rewrite the equation for w as a first order system using additional auxiliary functions to avoid high order derivatives.

Later on we will encounter some variations of these approximations. First of all, we will often find it convenient to write $A_j^{q_j}$ as a continued fraction rather than by a partial fraction expansion. The continued fraction representation seems to allow more directly an adaptive determination of q_j , though we have not yet implemented such a scheme. Second, it is possible to compute different exponential approximations to the kernels on different time intervals - a technique which is more general than the one we've outlined. Such a method is proposed in [80] and will be discussed in more detail below.

Local Approximations Already in [26] it was noted that Padé approximation produces boundary conditions which lead to well-posed problems. There the approximation was centered at normal incidence, which can also be thought of as an expansion of K_j valid for short time. We will follow the derivation due to Xu [104] which employs continued fractions.

To construct the approximations we note the relation:

$$\hat{K}_j(s) = \frac{\kappa_j^2}{2\frac{s}{c} + \hat{K}_j(s)}. \quad (21)$$

Then we define \hat{A}_j^q recursively:

$$\hat{A}_j^q = \frac{\kappa_j^2}{2\frac{s}{c} + \hat{A}_j^{q-1}}. \quad (22)$$

In [104] a number of choices for \hat{A}_j^0 are considered. For example, the choice $\hat{A}_j^0 = |\kappa_j|$ leads to spatially nonlocal conditions which are exact at steady-state, generalizing to high order the conditions of the type proposed in [25, 31]. Local conditions follow from the choice:

$$\hat{A}_j^0 = 0, \quad (23)$$

and may be written as the continued fraction (terminated after q terms with q independent of j):

$$\hat{A}_j^q = \frac{\kappa_j^2}{2\frac{s}{c} + \frac{\kappa_j^2}{2\frac{s}{c} + \frac{\kappa_j^2}{2\frac{s}{c} + \dots}}}. \quad (24)$$

To apply the approximate operator first define

$$w_0 = u, \quad w_k = A^{q+1-k} * w_{k-1}. \quad (25)$$

Here we have dropped the j dependence, as the multiplications by κ_j^2 may be replaced by applications of $-L$. Now the boundary condition approximating (9) is written in terms of:

$$w_1 = A^q * u. \quad (26)$$

We also have that

$$w_{q+1} = A^0 * w_q = 0. \quad (27)$$

We thus obtain the form:

$$\frac{\partial u}{\partial x} + \frac{1}{c} \frac{\partial u}{\partial t} + w_1 = 0, \quad (28)$$

$$\frac{2}{c} \frac{\partial w_k}{\partial t} = -Lw_{k-1} - w_{k+1}, \quad k = 1, \dots, q. \quad (29)$$

As a final step we reformulate the recursion so that only second order equations are solved. The details, along with first order reformulations suitable for incorporation into standard time-marching schemes, are found in [53]. Note that we are using the same symbols, w_k , to denote in general different auxiliary functions, except for w_1 . Also, we have assumed that $q = 2P$.

$$\frac{1}{c^2} \frac{\partial^2 w_1}{\partial t^2} = \frac{1}{2} L \frac{\partial u}{\partial x} + \frac{3}{4} L w_1 - \frac{1}{4} L w_2, \quad (30)$$

$$\frac{1}{c^2} \frac{\partial^2 w_k}{\partial t^2} = -\frac{1}{4} L w_{k-1} + \frac{1}{2} L w_k - \frac{1}{4} L w_{k+1}, \quad k = 2, \dots, P. \quad (31)$$

Again we emphasize the ease of applying this boundary condition to arbitrary order; it simply requires increasing the parameter P . We also note that the size of the final term, w_P , provides some measure of the error in terminating the fraction. If this measure could be made more precise, an adaptive implementation could be developed. The upcoming analysis and experiments will clarify the potential utility of an adaptive implementation. In particular we will see that the worst case analysis indicates that the necessary order could be quite large, while numerical experiments show that it is often possible to use a relatively low order.

To study the convergence of the method using (14) we must estimate:

$$\sup_{\Re s = \eta} \left| \frac{\kappa_j^2}{\frac{s}{c} + \left(\frac{s^2}{c^2} + \kappa_j^2\right)^{1/2}} - A_j^q(s) \right|. \quad (32)$$

Note that the branch points at $s = \pm i c \kappa_j$ make it difficult to derive good estimates when $\eta = 0$. Thus we accept $\eta > 0$. Estimates, derived in detail in [45, 104], follow recursively from the equation:

$$R^{q+1} = \frac{R^q}{(z + (z^2 + 1)^{1/2} + \kappa_j^{-2} R^q)(z + (z^2 + 1)^{1/2})}, \quad (33)$$

where

$$R^q = A_j^q(s) - \frac{\kappa_j^2}{\frac{s}{c} + \left(\frac{s^2}{c^2} + \kappa_j^2\right)^{1/2}}, \quad z = \frac{s}{c|\kappa_j|}. \quad (34)$$

Using (33) we find that the error is given by:

$$|R^q| \leq C \left(1 + \frac{\eta}{c|\kappa_j|}\right)^{-(2q+1)}. \quad (35)$$

As we must choose $\eta = O(T^{-1})$ to obtain a meaningful estimate, we find that to achieve a relative error tolerance of ϵ for the j th harmonic we require:

$$q = O(c|\kappa_j|T \ln \frac{1}{\epsilon}). \quad (36)$$

It is relatively straightforward to turn this into an estimate depending on various Sobolev norms of u on Γ . It tells us that for a fixed problem and fixed time that the method is spectrally convergent with increasing q . However, for $c|\kappa_j|T$ large many terms may be needed.

We note that to complete the convergence argument we must derive stability estimates. This is carried through in detail in [46, 104]. A complicating feature is the fact that the exact boundary conditions themselves do not satisfy the uniform Kreiss condition [73]. However, we can show that any growth of the stability constant with q is at worst linear, so that spectral convergence is retained. In our numerical experiments here and in [48] we have used very large values of $q > 100$ without observing any loss of stability.

To illustrate the stability and convergence of the local conditions we present the results of a simple numerical experiment. We solve the wave equation with $c = 1$ in the two-dimensional domain $(-2, 2) \times (0, 1)$ for $0 \leq t \leq 50$ with homogeneous Neumann boundary conditions on $y = 0, 1$. The initial data is generated by a Gaussian forcing at negative times which is shut off before $t = 0$. We use the boundary conditions (28), (30), (31), an eighth order two-step method in time and eighth order differencing in space. The spatial mesh was 264×66 and the number of time steps was 20000. Evaluating to high accuracy an integral formula for the exact solution, we are able to generate precise error data, which is shown in Figure 2. (The solution is $O(1)$ so that the absolute errors shown are comparable to relative errors.)

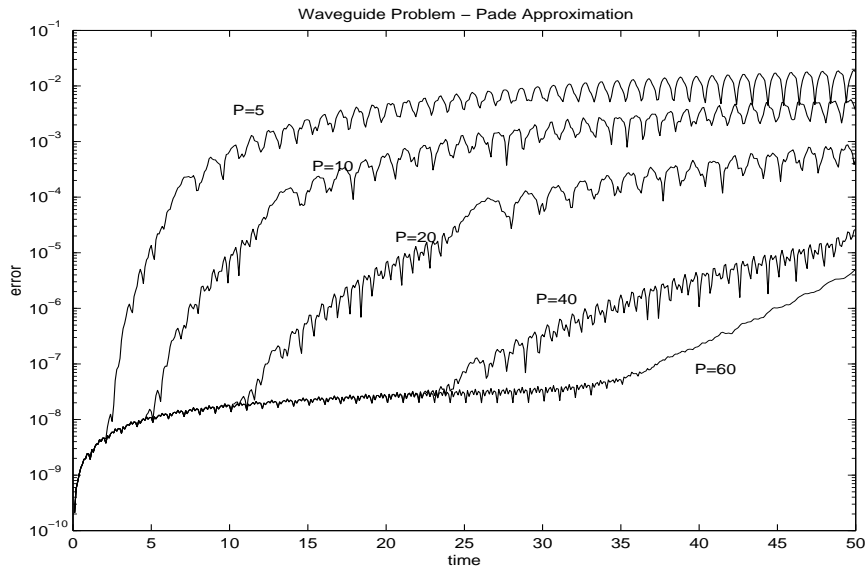


Fig. 2. Errors as a function of time and boundary condition order.

The results clearly show that the Padé approximation can be used to achieve excellent accuracy at modest cost. For example, $P = 20$ suffices for a tolerance of 10^{-3} up through $t = 50$. The results are also consistent with the error analysis. Note that we are plotting the total error due both to the

boundary approximations and the discretization, which limits the gains in accuracy which can be attained by increasing P alone. The stability of the conditions for P large are also confirmed.

We finally note that a number of other local approximations are possible. In [56] various alternatives are discussed, and a reasonable case is made that they should perform better. To implement them to high order, we note from [60, 61, 56] that they are formally equivalent to:

$$\prod_{k=1}^q \left(\frac{1}{c_k} \frac{\partial}{\partial t} + \frac{\partial}{\partial x} \right) u = 0, \quad 0 < c_k \leq c. \quad (37)$$

Directly, (37) can be difficult to implement. However, Givoli and Neta [35] and Guddati and Tassoulas [44] have recently shown how these can be reformulated using auxiliary functions. The precise result in [35] is that (37) is equivalent to:

$$\begin{aligned} \frac{\partial u}{\partial x} + \frac{1}{c_1} \frac{\partial u}{\partial t} + w_1 &= 0, & (38) \\ \left(\frac{1}{c_k} + \frac{1}{c_{k+1}} \right) \frac{\partial w_k}{\partial t} &= \left(\left(\frac{1}{c^2} - \frac{1}{c_k^2} \right) \frac{\partial^2}{\partial t^2} - L \right) w_{k-1} - w_{k+1}, \quad k = 1, \dots, q. & (39) \end{aligned}$$

In [44], on the other hand, a continued fraction interpolant of the wave speed function is directly computed, leading to a distinct but equivalent form, again without high order derivatives.

Clearly, (28)-(29) correspond to the special case $c_k = c$. The automatic optimization of these parameters as well as their application to more difficult problems are subjects with great potential. (Note that Higdon has applied his boundary conditions to a variety of problems, but not to high order [63, 64, 65].)

Spatially Nonlocal Approximations An unpleasant result of the preceding analysis is the poor behavior of the approximations for $|\kappa_j|T$ large. As shown in [46], this sort of long time behavior is to be expected from any homogeneous spatially local approximation. It is reasonable to ask how much better we can do if we allow spatially nonlocal conditions and construct norm-minimizing rational approximations.

Results along these lines have been obtained in [6]. Theoretically it is shown that a tolerance of ϵ can be met with:

$$q = O \left(\ln \frac{1}{\epsilon} + \ln c |\kappa_j| T \right), \quad (40)$$

which is clearly superior to (36). Near-optimal approximations were also constructed numerically using a nonlinear least squares procedure. (The resulting approximations are also accurate in the maximum norm as required by the error estimate.) For example, rational approximations are constructed in [6] satisfying the tolerances in Table 1.

ϵ	$c \kappa_j T$	q
10^{-4}	10^4	21
10^{-6}	10^4	31

Table 1. Number of poles required for various tolerances and times.

The rational function \hat{A}_j^q is expressed in partial fraction form:

$$\hat{A}_j^q = \kappa_j^2 \sum_{k=1}^q \frac{\alpha_k}{\frac{s}{c} - \beta_k |\kappa_j|}, \tag{41}$$

leading to the boundary condition

$$\frac{\partial u}{\partial x} + \frac{1}{c} \frac{\partial u}{\partial t} + \sum_{k=1}^q \phi_k = 0, \tag{42}$$

$$\frac{\partial \hat{\phi}_{jk}}{\partial t} - \beta_k |\kappa_j| \hat{\phi}_{jk} = \alpha_k \kappa_j^2 \hat{u}_j. \tag{43}$$

Note that the coefficients α_j and β_j are independent of c and κ_j and have been computed once and for all. In particular the poles lie strictly in the left half complex plane. (Their tabulated values can be downloaded from the address mentioned above.)

We have repeated the numerical experiment described above for the wave equation in a waveguide using (42),(43) instead of (28),(30),(31). An FFT, modified for the nonuniform mesh, is used to compute the direct and inverse Fourier series. Note that we use an eighth order quadrature rule to compute the transforms, so that if we use too many Fourier modes the accuracy is degraded. The results, shown in Figure 3, confirm the theoretical predictions. The errors when we use 16 modes are an order of magnitude smaller than the tolerances used to define the approximations themselves.

An alternative approach to constructing efficient nonlocal approximations has been proposed by Lubich and Schädle [80]. First, they reformulate the exact boundary condition using the Neumann-to-Dirichlet map (10). Second, they simplify the approximation problem somewhat by constructing local exponential approximations to the convolution kernels, $W_j(t)$, on time intervals:

$$I_l = (B^{l-1} \Delta t, (2B^l - 1) \Delta t), \tag{44}$$

where Δt is the time step employed in the discretization and B is an integer. (They recommend $B = 10$.) The positive result of this simplification is that they can construct effective approximations with predetermined pole locations, simply approximating the inverse Laplace transform by a quadrature rule on the so-called Talbot contour. Thus they can construct the approximations themselves far more rapidly than possible with the method used

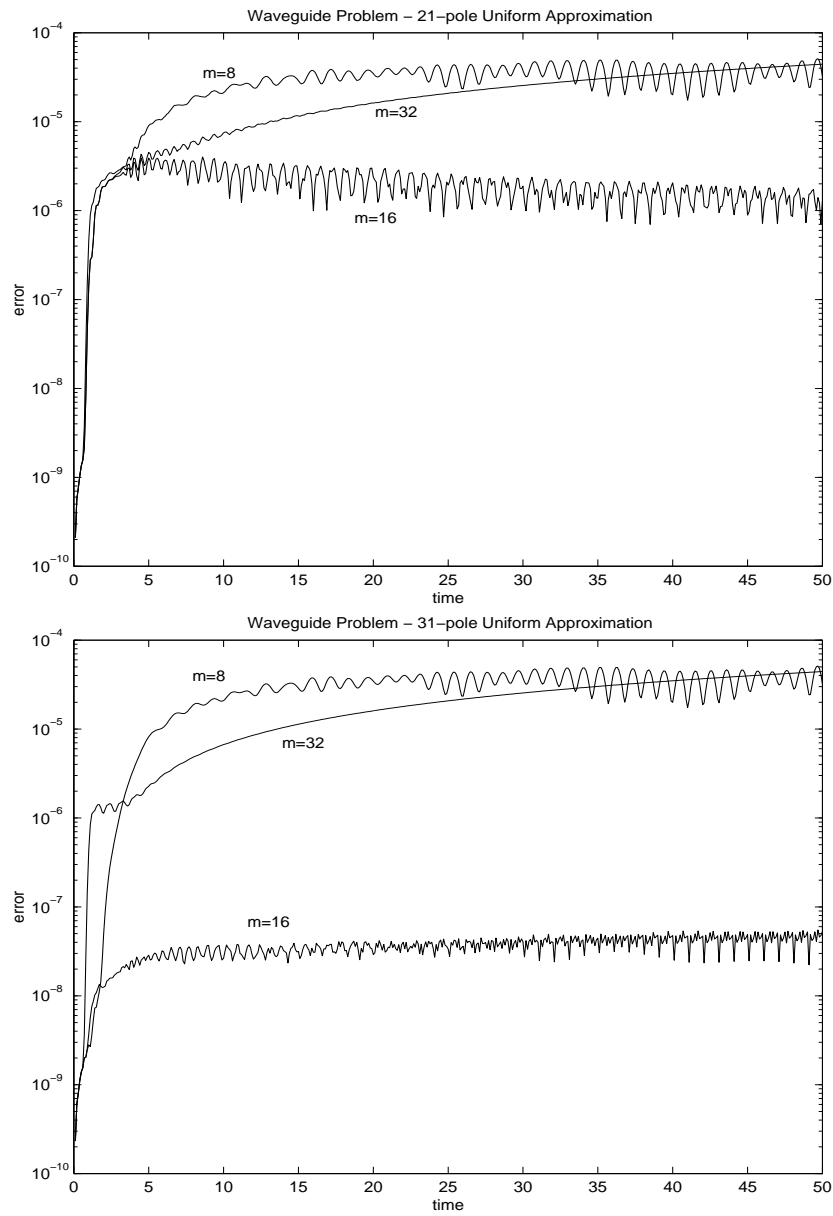


Fig. 3. Errors for the 21-pole and 31-pole least squares approximations. The parameter m is the number of Fourier modes used to evaluate the boundary condition.

in [5, 6]. This allows them to efficiently evaluate exact boundary conditions for the discretized problem, which can be more accurate when the solution is marginally resolved. On the negative side, the use of different approximations to the convolution kernel on different time intervals leads to a more complex implementation, and they require a little more work and storage than the method of [5, 6]. Precisely they require $O(\ln 1/\epsilon \cdot \ln c|\kappa_j|T)$ auxiliary functions.

2.2 The Wave Equation in an Exterior Domain

We now consider the wave equation in the second standard configuration for our class of problems, namely an exterior domain. Precisely, we suppose the tail, \mathcal{Y} , is such that $R^n - \mathcal{Y}$ is bounded and that within \mathcal{Y} the governing equation is:

$$\frac{1}{c^2} \frac{\partial^2 u}{\partial t^2} = \nabla^2 u, \quad x \in \mathcal{Y}. \quad (45)$$

We note that within the computational domain we may have inhomogeneities, nonlinearities, or any other perturbations.

Performing our usual Laplace transformation in time and supposing $\Re s$ sufficiently large (typically $\Re s > 0$) we are led to the problem of describing the trace on Γ of all bounded solutions of the Helmholtz equation:

$$\nabla^2 \hat{u} - \frac{s^2}{c^2} \hat{u} = 0. \quad (46)$$

A useful format for describing this trace is the Dirichlet-to-Neumann (or Neumann-to-Dirichlet) map, which we express as:

$$\frac{\partial \hat{u}}{\partial n} = D(s) \hat{u}, \quad x \in \Gamma. \quad (47)$$

(Precisely, we may define D if Γ is sufficiently smooth by solving the exterior Dirichlet problem with data \hat{u} and computing the trace of the normal derivative. Here $\partial/\partial n$ denotes the derivative into \mathcal{Y} , that is out of the computational domain.)

To derive concrete expressions for D it is necessary to restrict ourselves to simple boundaries, for example boundaries associated with coordinate systems in which the Helmholtz equation is separable. Even then there can be difficulties in transforming back to the time domain if the eigenfunctions of D are s -dependent. Thus the ideal case, from the point of view of analysis, is when Γ is chosen to be a sphere, and we will treat this case in great detail. However, the sphere is a wasteful choice for highly elongated or nonconvex scatterers. We will discuss some techniques which can be applied on high-aspect ratio or even nonconvex artificial boundaries. However, the problem of generalizing some of the more efficient and flexible methods remains open.

Assuming now that Γ is a sphere of radius R and expanding the solution of (46) in spherical harmonics:

$$\hat{u} = \sum_{l=0}^{\infty} \sum_{m=-l}^l \bar{u}_{lm}(r) Y_l^m(\theta, \phi), \quad (48)$$

we find that \bar{u}_{lm} satisfies:

$$\frac{\partial^2 \bar{u}_{lm}}{\partial r^2} + \frac{2}{r} \frac{\partial \bar{u}_{lm}}{\partial r} - \left(\frac{s^2}{c^2} + \frac{l(l+1)}{r^2} \right) \bar{u}_{lm} = 0. \quad (49)$$

The bounded solution of (49) is given by the modified spherical Bessel function:

$$\bar{u}_{lm}(r, s) = \frac{k_l(rs/c)}{k_l(Rs/c)} \bar{u}_{lm}(R, s), \quad (50)$$

$$k_l(z) = \frac{\pi}{2z} e^{-z} \sum_{k=0}^l \frac{(l+k)!}{k!(l-k)!} (2z)^{-k}. \quad (51)$$

To construct the Dirichlet-to-Neumann map we must compute the logarithmic derivative of k_l which from (51) is given by:

$$\frac{sk'_l(Rs/c)}{ck_l(Rs/c)} = -\frac{s}{c} - \frac{1}{R} - \frac{1}{R} \frac{\sum_{k=0}^{l-1} \frac{(2l-k)!}{k!(l-k-1)!} (2Rs/c)^k}{\sum_{k=0}^l \frac{(2l-k)!}{k!(l-k)!} (2Rs/c)^k}. \quad (52)$$

Summing over the harmonics and inverting the Laplace transform we finally find:

$$\frac{\partial u}{\partial r} + \frac{1}{c} \frac{\partial u}{\partial t} + \frac{1}{R} u + \frac{1}{R^2} \mathcal{H}^{-1} (S_l * (\mathcal{H}u)) = 0, \quad (53)$$

where \mathcal{H} denotes the spherical harmonic transform and the Laplace transform of S_l is given by the last term in (52).

The primary observation to be made is that \hat{S}_l is a rational function, albeit of degree $(l-1, l)$. Thus S_l can be written as a sum of exponential functions and, for each fixed harmonic, (53) can be localized in time. This fact was independently noticed by Sofronov [89, 90] and Grote and Keller [40, 41], who used it to construct temporally local boundary conditions which are exact on functions with finite harmonic content.

A second consequence of (50)-(51) is found by summing the series over l :

$$\hat{u} = \sum_{k=0}^{\infty} \frac{\pi}{(2rs/c)^{k+1}} e^{-rs/c} \sum_{l=k}^{\infty} \frac{(l+k)!}{k!(l-k)!} \sum_{m=-l}^l Y_l^m(\theta, \phi) \frac{\bar{u}_{lm}(R, s)}{k_l(Rs/c)}. \quad (54)$$

Defining:

$$\hat{f}_k(s/c, \theta, \phi) = \frac{\pi}{(2s/c)^{k+1}} \sum_{l=k}^{\infty} \frac{(l+k)!}{k!(l-k)!} \sum_{m=-l}^l Y_l^m(\theta, \phi) \frac{\bar{u}_{lm}(R, s)}{k_l(Rs/c)}, \quad (55)$$

and inverting the transform we produce the progressive wave or multipole expansion of u :

$$u = \sum_{k=0}^{\infty} \frac{f_k(ct-r)}{r^{k+1}}, \quad r \geq R. \quad (56)$$

Note again that if we assume finite harmonic content, $\bar{u}_{lm} = 0$ for $l > M$, then the series terminates with $k = M$.

From (56) we immediately derive the well-known Bayliss-Turkel conditions [16]:

$$\left(\frac{\partial}{\partial r} + \frac{1}{c} \frac{\partial}{\partial t} + \frac{2q+1}{R} \right) \cdots \left(\frac{\partial}{\partial r} + \frac{1}{c} \frac{\partial}{\partial t} + \frac{1}{R} \right) u = 0, \quad (57)$$

which we note are local and exact in the same sense as the conditions of [89, 90, 40, 41]. In the next section we will reformulate them using auxiliary functions to enable their high-order implementation.

Local Boundary Conditions Inspired by the reformulation of the Bayliss-Turkel conditions in [15], Hagstrom and Hariharan [49] gave the first reformulation of (57) in terms of auxiliary functions on Γ satisfying second order hyperbolic equations. Soon thereafter Huan and Thompson [70, 100] demonstrated the equivalence between the auxiliary functions of [49] and the residuals of the Bayliss-Turkel condition and also developed finite element implementations. Following them we set:

$$w_{k+1} = \left(\frac{\partial}{\partial r} + \frac{1}{c} \frac{\partial}{\partial t} + \frac{2k+1}{R} \right) \cdots \left(\frac{\partial}{\partial r} + \frac{1}{c} \frac{\partial}{\partial t} + \frac{1}{R} \right) u. \quad (58)$$

Obviously,

$$\left(\frac{\partial}{\partial r} + \frac{1}{c} \frac{\partial}{\partial t} + \frac{2k+1}{R} \right) w_k = w_{k+1}, \quad (59)$$

and (57) is equivalent to:

$$\left(\frac{\partial}{\partial r} + \frac{1}{c} \frac{\partial}{\partial t} + \frac{1}{R} \right) u = w_1, \quad w_{q+1} = 0, \quad (60)$$

combined with (59). The only problem with this formulation is the presence of the radial derivative in (59), which would force us to define the auxiliary functions in the interior. To eliminate it we note the identity derived in [70], which can easily be proven by induction:

$$\left(\frac{\partial}{\partial r} - \frac{1}{c} \frac{\partial}{\partial t} + \frac{1}{r} \right) w_k = -\frac{1}{r^2} (\nabla_{\Gamma}^2 + k(k-1)) w_{k-1}, \quad (61)$$

where ∇_{Γ}^2 denotes the Laplace-Beltrami operator on the sphere:

$$\nabla_{\Gamma}^2 w = \frac{1}{\sin \theta} \frac{\partial}{\partial \theta} \left(\sin \theta \frac{\partial w}{\partial \theta} \right) + \frac{1}{\sin^2 \theta} \frac{\partial^2 w}{\partial \phi^2}. \quad (62)$$

Using (61) to eliminate $\frac{\partial w_k}{\partial r}$ from (59) we obtain our desired system:

$$\left(\frac{1}{c} \frac{\partial}{\partial t} + \frac{k}{R}\right) w_k = \frac{1}{2R^2} (\nabla_{\Gamma}^2 + k(k-1)) w_{k-1} + \frac{1}{2} w_{k+1}. \quad (63)$$

Equations (63) together with (60) are our final reformulation of (57). We again remark that they are easily implemented to any order by introducing additional auxiliary functions, that is by increasing q , and retain the property of being exact on functions described by harmonics of index up through q . We also note their obvious similarity to the planar boundary conditions based on the Padé approximation, (28)-(29). (The difference in scalings corresponds to a different scaling of the auxiliary functions.)

We have not yet carried through a complete convergence proof for these boundary conditions for fixed R and increasing q . We note that if we write:

$$u = u^{(q)} + \delta^{(q)}, \quad (64)$$

where $u^{(q)}$ is the projection of u onto the span of the harmonics of index up through q , then the consistency error is simply the result of applying the boundary condition to $\delta^{(q)}$. Moreover, for smooth solutions $\|\delta^{(q)}\|_{L_2}$ decays to zero faster than any power of q . Thus it is reasonable to conjecture that the proposed conditions are spectrally convergent uniformly in time.

An analogous sequence of boundary conditions can be constructed on circular boundaries in two space dimensions (and cylindrical boundaries in three). However, unlike the three-dimensional case, we have no expectation of time-uniform convergence. Indeed, the results of [50] essentially preclude it. In [53] we show how to rewrite these conditions so that only first order derivatives of the auxiliary functions appear, implement the conditions in a discontinuous Galerkin spectral element code for Maxwell's equations [59], and carry out numerical experiments. In Figure 4 we plot the error over time for a two-dimensional simulation of a TE-pulse. Clearly the results are analogous to those obtained in the plane case, noting that for the waveguide experiments the solution was better resolved. (Compare with Figure 2.)

In addition to the applications to Maxwell's equations in [53], some other generalizations of this method have recently been completed. In [51] boundary conditions analogous to (60),(63) are constructed for the convective wave equation,

$$\left(\frac{\partial}{\partial t} + M \frac{\partial}{\partial x}\right)^2 u = \nabla^2 u, \quad (65)$$

where $0 < M < 1$ is the Mach number. These will be applicable to problems governed by the linearized subsonic Euler equations in \mathcal{Y} . Generalizations to the wave equation in a layered half space, motivated by problems in soil-structure interaction, have also been proposed [105].

A defect of the preceding analysis from the point of view of certain applications is the fact that the underlying expansion (56) only holds exterior

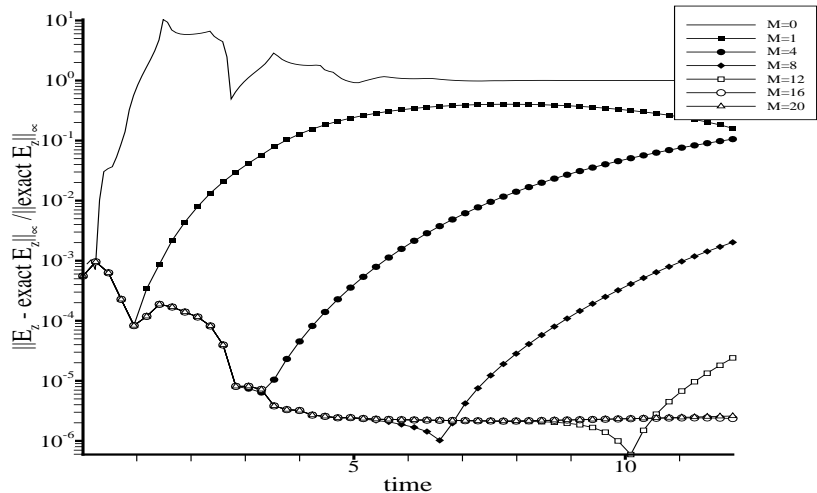


Fig. 4. Errors as a function of order, M , and time. Reformulated cylindrical Bayliss-Turkel condition. DG Maxwell solver.

to a sphere containing the problem’s inhomogeneities. This could be quite wasteful of computational volume for problems with very high aspect ratio scatterers. (This defect is shared by many of the nonlocal formulations we will discuss below.) This suggests that it could be useful to find an alternative expansion with a convergence domain exterior to a high-aspect ratio boundary, which would serve as Γ . For the Helmholtz equation, Holford [67] has constructed such an expansion with Γ an oblate or prolate spheroid. Translated to the time domain, the results in [67] suggest that (56) holds exterior to a spheroid with the r coordinate replaced by its analogues in the relevant spheroidal coordinate system. On this basis we believe that a sequence of boundary conditions generalizing (60),(63) could be constructed which might prove efficient for a large class of problems. We also note that related methods based on spheroidal infinite elements have been considered [8, 9, 10].

A second approach to efficiently bounding a high-aspect ratio scatterer is to use a rectangular box, applying conditions such as (28), (30),(31) or (38),(39) on each face. There are two issues which must be considered in this context. First, it is necessary to provide some boundary conditions at the edges which relate the auxiliary functions on adjacent faces. Second, it is necessary to develop some argument that the approximations will converge with increasing q .

In [102], Vacus makes substantial progress on the first issue. Considering the boundary conditions (37), he proves the existence of a unique smooth solution in the rectangular domain assuming sufficiently regular data. He also describes an algebraic procedure for deriving corner compatibility conditions. Vacus' construction involves taking high order space-time derivatives of both the equations and the boundary conditions and finding linear combinations which can be integrated to yield nontrivial constraints. It will take some additional effort to translate his results into usable compatibility relations for our preferred auxiliary variable formulations. We note that earlier Collino [18] derived corner compatibility relations for an auxiliary variable formulation of the boundary conditions based on Padé approximations. He used a sequence of exact solutions of the wave equation to determine the relations. As it is not obvious how to generalize either construction to more complex situations, a new and somewhat more straightforward approach would be very useful.

Vacus' uniqueness theorem lends some credence to the belief that the method will converge. In particular, convergence on the planes containing each face follows from the results above, and the corner compatibility conditions should lead to auxiliary functions which agree with the restrictions of the planar auxiliary functions. However, this argument is far short of a proof. Thus a definitive analysis of convergence for rectangular T would be an important advance. Note that it is plausible that the error estimates will be better than for the plane. The nonuniformity in time is due to the possibility of late-time glancing incidence. However, waves which impinge on one part of the boundary at glancing angles impinge on other parts nearly normally, and thus are very well-absorbed.

Nonlocal Conditions Nonlocal boundary conditions for exterior problems have been constructed from at least three distinct formulations of exact boundary conditions. The most straightforward are based on the evaluation of (53). Directly, Grote and Keller [40, 41] compute some (typically small) number of spherical harmonic expansion coefficients and solve a system of ordinary differential equations equivalent to the order l system defined by \hat{S}_l . For l large, however, this method (and the companion local methods described earlier) require a large number of auxiliary variables. This number can be significantly reduced if least squares approximations are used instead. Note in this case we are approximating the degree $(l-1, l)$ rational function, \hat{S}_l , by a rational function of lower degree, (q_l-1, q_l) . A fundamental theoretical result of [5] is that for an absolute error tolerance ϵ we can take:

$$q_l = O(\ln l + \ln 1/\epsilon). \quad (66)$$

Note that, unlike the case of a plane boundary, this estimate is uniform in time. That is, we can approximate \hat{S}_l on the imaginary axis.

In either case, the nonlocal term in (53) is replaced by an expression of the form:

$$\frac{1}{R^2} \sum_{l=0}^P \sum_{m=-l}^l Y_l^m(\theta, \phi) \sum_{k=1}^{q_l} \phi_{lmk}, \quad (67)$$

with the auxiliary functions satisfying ordinary differential equations. For example, using the representation from [5, 6]:

$$\frac{1}{c} \frac{\partial \phi_{lmk}}{\partial t} + \frac{1}{R} \beta_{lk} \phi_{lmk} = \alpha_{lk} \tilde{u}_{lm}, \quad (68)$$

where $\tilde{u}_{lm}(t)$ is a coefficient in the spherical harmonic expansion of u on Γ .

The nonlinear least squares procedure has also been employed to compute the pole locations and strengths for near-optimal approximations. That is, we have computed q_l and the complex numbers α_{lk} , β_{lk} for the spherical version of (68). (They can be obtained from the website mentioned earlier.) In Table 2 we list the number of poles, and thus the number of auxiliary functions, needed for each harmonic with $\epsilon = 10^{-8}$ for both the sphere and cylinder kernels. We note that the numbers are very small - no more than 21-poles per harmonic are needed to guarantee excellent time-uniform accuracy for harmonics up through index 1024. By way of comparison, the methods of [89, 90, 40, 41, 49] would all require 1024 to be exact for such modes. Thus for a difficult problem with high harmonic content at the boundary it clearly pays to use the least squares approximations. The primary cost associated with the application of the boundary condition is the computation of the direct and inverse spherical harmonic transformations. Mohlenkamp [81], Suda and Takami [92], and Healy and coworkers [57] have devised fast algorithms for this purpose. Using them, the formal operation count for applying the boundary condition is of much lower order than the count associated with the interior solve, though for moderate size problems asymptotically more complex methods can be faster. Tables of poles and amplitudes can be downloaded from the web site mentioned above.

The cost of the spherical harmonic transform aside, the efficiency of the least squares approximations in the spherical case is unmatched. However, just as the sequences of local boundary conditions, their current formulation requires a spherical (cylindrical) artificial boundary, which is an expensive choice for a high-aspect ratio scatterer. Possible solutions, again just as in the local case, are to extend the construction to spheroids or boxes. A problem here is that exact conditions on these boundaries are fundamentally more complex. In particular, they can not be diagonalized by a fixed spatial basis. We feel that the development of efficient representations of boundary conditions on high-aspect ratio surfaces is an important problem which should be studied further.

The other two nonlocal formulations both allow for the flexible choice of Γ , but are otherwise more costly. The first, suggested in [101], is based on a formulation of exact boundary conditions using retarded potentials. It involves enclosing the scatterer by two surfaces, Γ_I and Γ_O , as indicated in Figure 5.

\hat{C}_l		\hat{S}_l	
l	q_l	l	q_l
0	44		
1	15		
2	9		
3- 8	7	0- 7	l
9- 10	8	8- 10	8
11- 14	9	11- 14	9
15- 20	10	15- 19	10
21- 28	11	20- 28	11
29- 41	12	29- 40	12
42- 58	13	41- 57	13
59- 84	14	58- 83	14
85- 123	15	84- 123	15
124- 183	16	124- 183	16
184- 275	17	184- 275	17
276- 418	18	276- 418	18
419- 638	19	419- 637	19
639- 971	20	638- 971	20
972-1024	21	972-1024	21

Table 2. Number of poles needed to approximate the exact boundary condition kernels to an accuracy of 10^{-8} . From [5].

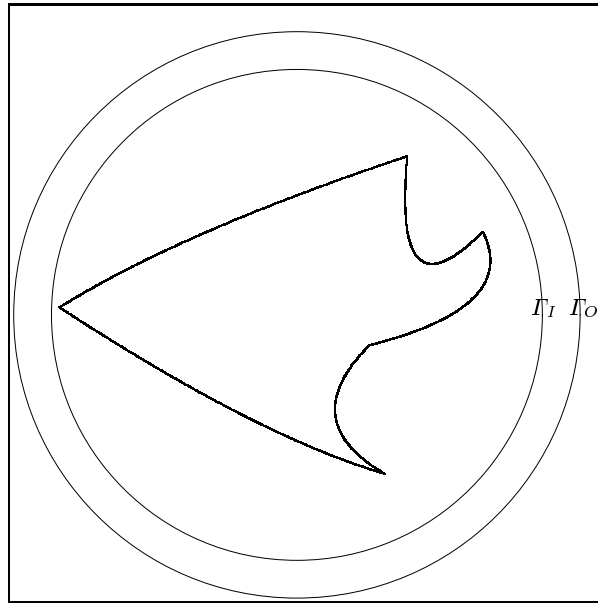


Fig. 5. A domain configurations with two boundaries.

Then we can evaluate u on Γ_O using past values of u and its derivatives on Γ_I . Precisely:

$$u(x, t) = -\frac{1}{4\pi} \int_{\Gamma_I} \left(u \frac{\partial}{\partial n} \left(\frac{1}{r} \right) - \frac{1}{r} \frac{\partial u}{\partial n} - \frac{1}{rc} \frac{\partial r}{\partial n} \frac{\partial u}{\partial t} \right) dy, \quad (69)$$

where $x \in \Gamma_O$, $\partial/\partial n$ is the normal derivative, $r = |x - y|$ and the time argument of u in the integral is $t - r/c$. We note that although the formula is nonlocal in time, the required history extends over only a finite interval determined by the maximum travel time between points on the boundary.

The first implementation of (69) appears in [34]. However, it employs a direct numerical evaluation of the integral, which implies a cost per time step proportional to the square of the number of boundary points. This is more costly by one order than the interior solve, and is thus not competitive with other methods. Recently, a fast algorithm for evaluating retarded potentials has been devised [28]. Using this algorithm, the formal operation count associated with (69) becomes comparable to the counts for the methods described above, though in practice it is still quite expensive. However, the method is competitive in certain special cases, for example for highly nonconvex scatterers.

The final method, due to Ryaben'kii and coworkers [86, 87], is based directly on the strong Huygens' principle (or the existence of lacunae) which itself follows from (69). As a first step, consider again Figure 5 and introduce a smooth cutoff function, $\zeta(x)$, satisfying $\zeta = 1$ at and beyond Γ_O and $\zeta = 0$ inside Γ_I . Introducing the auxiliary function:

$$v = \zeta u, \quad (70)$$

we see that v satisfies a forced wave equation in all space:

$$\frac{1}{c^2} \frac{\partial^2 v}{\partial t^2} = \nabla^2 v + f, \quad x \in R^3, \quad (71)$$

where f is supported between Γ_O and Γ_I . Since $u = v$ on Γ_O , an exact Dirichlet boundary condition can be imposed if a solution of (71) can be computed. To solve (71) we note that if f is supported only in the time interval (t_j, t_{j+1}) , the strong Huygens' principle would imply that $v \neq 0$ on Γ_O only on some larger time interval, (t_j, T_{j+1}) . Moreover, on this time interval, v restricted to Γ_O is identical to the solution of a periodic problem in space with sufficiently large period.

The algorithm proposed in [87] is based on these observations. By a smooth partition of unity in time, f is written as the sum of functions, f_j , which are supported on time intervals of fixed duration. Then v on Γ_O is written as the sum of functions v_j which solve spatially periodic wave equations with forcing f_j . The periodic spatial domains must be chosen fairly large - larger than the domains required by a spherical artificial boundary. However,

the equation for the functions v_j is simple and can be very efficiently solved using a Fourier spectral method. Thus the resulting algorithm is competitive.

We finally mention an intriguing result of Warchall [103]. He proves that if u solves the wave equation, with all inhomogeneities and initial data supported inside a convex domain, Ω , bounded by Γ , the solution at times $t \geq t_p \geq 0$ is completely determined by the data within $\Omega \cap B(x, c(t - t_p))$ at time t_p . This seems to imply that an exact boundary condition with no history dependence or auxiliary variables exists. However, to date this exact operator has not been found.

2.3 First Order Hyperbolic Systems

We now return to the case of a cylindrical tail, $\mathcal{Y} = (0, \infty) \times \Xi$. However we assume that Ξ is rectangular and that the equation in \mathcal{Y} is the first order, constant coefficient hyperbolic system:

$$\frac{\partial u}{\partial t} = A \frac{\partial u}{\partial x} + \sum_j B_j \frac{\partial u}{\partial y_j} + Cu, \quad (72)$$

where the diagonal matrix A is partitioned into incoming and outgoing pieces. (We are assuming that $x = 0$ is noncharacteristic, but that assumption can be relaxed.)

$$A = \begin{pmatrix} A^+ & O \\ O & A^- \end{pmatrix}, \quad A^+ > O, \quad A^- < O. \quad (73)$$

We also suppose that appropriate boundary conditions are imposed on $\partial\Xi$. After a Fourier-Laplace transformation, we derive the system of equations in x :

$$\frac{\partial \bar{u}}{\partial x} = A^{-1} \left(sI - \sum_j ik_j B_j - C \right). \quad (74)$$

For any fixed transverse mode, this system clearly possesses an exponential dichotomy for $\Re s$ sufficiently large. Moreover, the dimension of the subspace of growing solutions is that of A^+ . An exact boundary condition is then given by:

$$P^+(s, k) \bar{u} = 0, \quad (75)$$

where P^+ is a projector into the subspace of growing solutions. Noting further that in the large s limit this equation reduces to $u^+ = 0$ we reach our final form:

$$u^+ = \mathcal{F}^{-1} (R(t, k) * (\mathcal{F}u)), \quad (76)$$

where R is now a matrix.

We note first that the projection operator is not unique and not every choice leads to a well-posed problem. For example, the obvious choice of left eigenvectors to define P^+ leads to an ill-posed problem for the linearized, subsonic Euler equations [32, 48]. Second, we have restricted the cross-section

to a rectangle so that we could reduce the problem to a linear algebra problem using Fourier series. More generally the projection onto outgoing waves (decaying solutions after Laplace transformation) is more difficult. Finally, even if we can reduce the problem to linear algebra, we may be unable to find analytic representations of the projectors.

Despite these difficulties, there are a number of important examples where we can make progress. Not surprisingly, in each of these cases the basic propagating modes either satisfy the wave equation or the simple transport equation. Below we will discuss two such cases in some detail, Maxwell's equations and the linearized Euler equations. Other systems which can be discussed include the linearized shallow water equations, which are closely related to the Euler equations, and the equations of linear elasticity, which are typically formulated as a second order system. For a treatment of the latter see [83, 62, 63, 39, 43].

Maxwell's Equations Maxwell's equations in free space using appropriate units are given by:

$$\frac{1}{c} \frac{\partial E}{\partial t} - \nabla \times B = 0, \quad (77)$$

$$\frac{1}{c} \frac{\partial B}{\partial t} + \nabla \times E = 0. \quad (78)$$

Systematic derivations of exact boundary conditions can be found in [42, 47]. Here we'll take a shortcut, noting that each of the Cartesian components of the field vectors satisfies the scalar wave equation. Thus, we can use the boundary conditions discussed above to eliminate the normal derivatives of any variable. We simply use the normal characteristic analysis to predict which variables we need to specify. Note that for Maxwell's equations there are, at any boundary, two incoming, two outgoing and two characteristic variables. Thus we will impose two boundary conditions. See [53] for more details and numerical experiments with local conditions.

In our waveguide geometry, where x is the normal coordinate and (y, z) the tangential coordinates, the incoming normal characteristic equations are:

$$\left(\frac{1}{c} \frac{\partial}{\partial t} - \frac{\partial}{\partial x} \right) (E_y - B_z) + \frac{\partial E_x}{\partial y} - \frac{\partial B_x}{\partial z} = 0, \quad (79)$$

$$\left(\frac{1}{c} \frac{\partial}{\partial t} - \frac{\partial}{\partial x} \right) (E_z + B_y) + \frac{\partial E_x}{\partial z} + \frac{\partial B_x}{\partial y} = 0. \quad (80)$$

Using (9) to eliminate the x -derivatives yields the exact boundary condition:

$$\left(\frac{2}{c} \frac{\partial}{\partial t} + \mathcal{F}^{-1} \circ (K_j^*) \circ \mathcal{F} \right) (E_y - B_z) + \frac{\partial E_x}{\partial y} - \frac{\partial B_x}{\partial z} = 0, \quad (81)$$

$$\left(\frac{2}{c} \frac{\partial}{\partial t} + \mathcal{F}^{-1} \circ (K_j^*) \circ \mathcal{F} \right) (E_z + B_y) + \frac{\partial E_x}{\partial z} + \frac{\partial B_x}{\partial y} = 0. \quad (82)$$

Finally, we can replace the exact nonlocal term by either the local sequences or the nonlocal least squares approximations.

A similar procedure can be carried out on a sphere. Each Cartesian component of the fields satisfies (53). One simply writes the equations for the incoming variables at each point and replaces r derivatives using (53) and whatever local or nonlocal approximation to the nonlocal term, $\mathcal{H}^{-1}(S_t * (\mathcal{H}u))$, is chosen. As described, this method would require the definition of auxiliary functions for all six components. However, the more complex derivations in [42, 47] show that only two sets are required.

Linearized Euler Equations As a second example, consider the compressible Euler equations linearized about a uniform, subsonic flow:

$$\frac{D\rho}{Dt} + \nabla \cdot u = 0, \quad (83)$$

$$\frac{Du}{Dt} + \frac{1}{\gamma} \nabla p = 0, \quad (84)$$

$$\frac{Dp}{Dt} + \gamma \nabla \cdot u = 0. \quad (85)$$

Here the material derivative is defined by:

$$\frac{D}{Dt} \equiv \frac{\partial}{\partial t} + U \cdot \nabla, \quad (86)$$

and U is the uniform flow field about which we've linearized. Note that units have been chosen so that the sound speed is one. Thus:

$$\sum_{j=1}^3 U_j^2 = M^2 < 1. \quad (87)$$

We also assume $U_1 > 0$.

The linearized Euler equations support waves of differing types. Combining (84) and (85) we find that the pressure, p , satisfies the convective wave equation:

$$\frac{D^2 p}{Dt^2} = \nabla^2 p. \quad (88)$$

On the other hand, the entropy, $S = p - \gamma\rho$, and the vorticity, $\omega = \nabla \times u$ satisfy the transport equation:

$$\frac{DS}{Dt} = 0, \quad \frac{D\omega}{Dt} = 0. \quad (89)$$

Thus the boundary condition problem for the pressure is similar to the boundary condition problem for the wave equation. Indeed, we have shown in [48, 51] that the local boundary condition sequences discussed above for

both waveguide and exterior geometries can be generalized to the convective wave equation. In addition, exact boundary conditions for (89) are extremely simple; namely:

$$S = 0, \quad \omega = 0, \quad \text{if } U \cdot n < 0, \quad (90)$$

where U is the outward normal - that is if the flow is incoming. The primary difficulty is to combine these relationships to produce a well-posed problem at inflow.

In [48] the full range of well-posed formulations of exact boundary conditions is displayed. (See also [91, 84].) At outflow, where there is a single incoming acoustic mode, the boundary condition is essentially uniquely defined:

$$\frac{D_{\text{tan}}}{Dt}(p - u_1) + \mathcal{K}p + U_1 \left(\frac{\partial u_2}{\partial x_2} + \frac{\partial u_3}{\partial x_3} \right) = 0, \quad (91)$$

At inflow there are many possibilities. The simplest realization, which is used in the numerical experiments, is:

$$\gamma\rho - p = 0, \quad (92)$$

$$\frac{D_{\text{tan}}}{Dt}(p + u_1) + \frac{1}{2}\mathcal{K}(p + u_1) + \frac{1 - U_1}{2} \left(\frac{\partial u_2}{\partial x_2} + \frac{\partial u_3}{\partial x_3} \right) = 0, \quad (93)$$

$$\frac{D_{\text{tan}}u_2}{Dt} + U_1 \frac{\partial u_1}{\partial x_2} + \frac{\partial p}{\partial x_2} = 0, \quad (94)$$

$$\frac{D_{\text{tan}}u_3}{Dt} + U_1 \frac{\partial u_1}{\partial x_3} + \frac{\partial p}{\partial x_3} = 0. \quad (95)$$

Here, \mathcal{K} denotes a nonlocal operator very closely related to the operator appearing in (9). Precisely:

$$\mathcal{K}w = \mathcal{F}^{-1} \left((1 - U_1)^2 k^2 K(\sqrt{1 - U_1^2} kt) * (\mathcal{F}w) \right), \quad (96)$$

where $K(\kappa_j t)$ is the kernel we had before. In particular, both the local and nonlocal approximations we have discussed can be used here. In [48], for example, we use the Padé sequence for a problem involving a periodic array of pressure pulses. The results are similar to those reported in Figure 2.

As mentioned above, it is also possible to generalize the local boundary condition sequence we have discussed from the wave equation to the convective wave equation [51]. However, we have yet to complete the construction of a well-posed inflow condition. We note that for the exterior problem a smooth artificial boundary must contain a point where $U \cdot n = 0$. Thus the switch between inflow and outflow conditions may require some additional compatibility conditions for the auxiliary variables. Given the importance of compressible flow problems, the resolution of this issue is certainly important.

Variable Coefficients and General Systems We've now completed the list of hyperbolic problems which we can satisfactorily solve. Although it contains many of the more important equations arising in applications, it certainly doesn't contain them all. Particularly glaring is our inability to treat variable coefficient problems and general hyperbolic systems.

We note that in their original work [27], Engquist and Majda do treat the variable coefficient case from the perspective of the reflection of singularities. More recently, practical algorithms for constructing the Engquist-Majda conditions to high order have been proposed [7]. However, the underlying expansions are only convergent up to smooth errors, which may not be small. Thus, unless a stronger form of convergence can be established for some cases, it is not obvious that high order constructions will be useful. (We note that a sort of convergence has been established in the highly oscillatory limit in [55] for the lowest order Engquist-Majda conditions.)

A second approach to these issues is the reformulation of Higdon's boundary conditions in [35, 36]. Already in their original version applications to problems in stratified media have been undertaken [64]. For problems with traveling waves only, the input to the method is simply a range of wave speeds which can, in principle, be estimated from the coefficients. However, the reformulations currently require a second order system and need to be generalized to the first order case. Moreover, modal solutions to variable coefficient problems may be growing or decaying and it is unclear if the conditions need to be reformulated in that case. In any event, we believe the method has great promise, but it is clear that much more experimentation and analysis is needed.

2.4 The Schrödinger Equation

Waves, particularly dispersive waves, can also be described by higher order equations. Work on these systems is less well-developed, though low order conditions of Higdon type have certainly been used. In recent years, however, there have been advances in the treatment of the most important equation from this class, the Schrödinger equation. In particular, two recent dissertations, by Jiang at NYU [72] and Schädle in Tübingen [88] deal with the construction, analysis and testing of highly accurate nonlocal conditions. (See also [80].)

We begin again with the case of a cylindrical tail:

$$-i \frac{\partial u}{\partial t} = \frac{\partial^2 u}{\partial x^2} + L(y, \partial / \partial y) u. \quad (97)$$

Expanding in a Fourier series in the cross-section based on the eigenfunctions of L and performing a Laplace transform in time we obtain a formula for an exact boundary condition:

$$\frac{\partial \hat{u}_j}{\partial x} + (-is + \kappa_j^2)^{1/2} \hat{u}_j = 0. \quad (98)$$

We immediately note an important difference between (98) and its wave equation analogue. To derive boundary conditions for the wave equation, we simply removed the large s behavior from the nonlocal term until the remaining operator was equivalent to convolution with a bounded function. As for large s the symbol was linear, the total operator was the sum of a differential operator and the convolution. Here, in contrast, the symbol behaves like $(is)^{1/2}$ for s large. To desingularize this somewhat, we can use the Neumann-to-Dirichlet map as in [88, 80],

$$\mathcal{F}^{-1} \left(V_j * \left(\mathcal{F} \frac{\partial u}{\partial x} \right) \right) + e^{-i\frac{\pi}{4}} u = 0, \quad (99)$$

or, as in [72], write:

$$(-is + \kappa_j^2)^{1/2} = e^{-i\frac{\pi}{4}} \frac{(s + i\kappa_j^2)}{(s + i\kappa_j^2)^{1/2}}, \quad (100)$$

leading to:

$$\frac{\partial u}{\partial x} + e^{-i\frac{\pi}{4}} \mathcal{F}^{-1} \left(V_j * \left(\mathcal{F} \left(\frac{\partial u}{\partial t} - iLu \right) \right) \right) = 0. \quad (101)$$

In either case, the boundary condition is expressed in terms of convolution with:

$$V_j(t) = \mathcal{L}^{-1}(s + i\kappa_j^2)^{-1/2} = \frac{e^{-i\kappa_j^2 t}}{\sqrt{\pi t}}. \quad (102)$$

Unlike the kernels we dealt with earlier, the singularity at $t = 0$ precludes the uniform approximation of V_j on $(0, \infty)$. Thus both authors split the convolution into two pieces, a local piece on $(0, \delta)$ to be handled by direct discretization, and a global piece where V_j is replaced by exponential or piecewise exponential functions. Jiang's global approximation is based on approximating the integral formula:

$$\frac{1}{\sqrt{\pi t}} = \frac{2}{\pi} \int_0^\infty e^{-z^2 t} dz, \quad (103)$$

and leads to the estimate:

$$q_l = O(\ln 1/\epsilon \cdot (\ln T/\delta + \ln \ln 1/\epsilon)). \quad (104)$$

Lubich and Schädle, on the other hand, use the same algorithm they suggest for kernels arising from the wave equation. They require about the same number of poles, though the implementation is more complex. They do treat the discretized problem, however.

Similarly, exact boundary conditions can be formulated on spherical and cylindrical boundaries. Transforms of the resulting kernels are still expressed

by logarithmic derivatives of modified Bessel functions, but now the arguments are proportional to $s^{1/2}$. Theoretically, Jiang shows that the approximation theorems of [5] can be applied in this case, precisely to:

$$\mathcal{L}^{-1} \left(\frac{\sqrt{is} K'_\nu(\sqrt{is})}{(s - s_\nu) K_\nu(\sqrt{is})} \right). \quad (105)$$

(A multiplication and division by $s - s_\nu$ has been performed to regularize the kernel.) Choosing δ as above he shows that for harmonics of index l the number of poles required is:

$$q_l = O((\ln 1/\epsilon + \ln 1/\delta) \cdot (\ln l + \ln 1/\epsilon + \ln 1/\delta)). \quad (106)$$

Actual approximations are also computed in [72] by a least squares procedure. Generally, more poles are required than for the simpler case of the wave equation. Nonetheless, these nonlocal approximations do provide arbitrary accuracy at relatively small cost. Moreover, high-order local alternatives do not as yet exist.

As an example of the difficulties in constructing high-order local boundary conditions for the Schrödinger equation, we point to the recent paper of Allonso-Mallo and Reguera [4], where they study the stability of Higdon-type boundary conditions proposed for the Schrödinger equation in [29, 24]. They find mild instabilities which worsen with increasing order for semidiscretizations of the problem. Their analysis ends at rather low order by our standards - a rational approximation of degree (3, 2). It leads to doubt about the utility of very high order conditions, though this still needs to be tested.

3 Absorbing Layers

The alternative to domain truncation by accurate boundary conditions is the use of an absorbing or sponge layer. The idea is simple - extend the computational domain from the boundary of the physical domain, Γ_I , to a second boundary, Γ_O , and change the equations in the new buffer zone so that waves decay. It is obviously not difficult to write down dissipative wave equations whose solutions decay rapidly as they propagate. However, impinging waves generally reflect off the interface or transition zone and thus return to Ω . As a result, early methods of this type (e.g. [71]) required a gradual increase in the absorption parameters, leading to fairly thick layers. All of this changed with Bérenger's introduction of the perfectly matched layer (PML) for Maxwell's equations [14].

The new property of the PML is a reflectionless interface with the physical domain. In the original paper, the origins of this property are somewhat obscured. However, soon thereafter it was noted that the PML was

in fact equivalent to a continuation into the complex plane of the real, normal coordinate, for example x for our cylinder domains [17]. This observation has led to a number of important generalizations to curvilinear coordinates [94, 20, 96, 82], which we'll discuss below, and to more complex media [95, 97, 98]. We will present a nonstandard derivation of the PML which generalizes the coordinate transformation approach. A result of this generalization has been the extension of the PML to the linearized Euler equations. Interestingly, in this framework the reflectionless interface property is easily satisfied, but the dissipativity condition is not.

3.1 Perfectly Matched Layers for Hyperbolic Systems

Consider our usual cylindrical tail and suppose we are solving a first order hyperbolic system which we allow to have varying coefficients in the cross section;

$$\frac{\partial u}{\partial t} + A(y) \frac{\partial u}{\partial x} + \sum_j B_j(y) \frac{\partial u}{\partial y_j} + C(y)u = 0. \quad (107)$$

Just as before, the physical domain is located in $x < 0$, the interface, Γ , between the physical domain and the absorbing region is located at $x = 0$, and the absorbing region itself lies between $x = 0$ and $x = L$.

Performing a Laplace transformation in time we find modal solutions of (107):

$$\hat{u} = e^{\lambda x} \phi, \quad (108)$$

where

$$\left(sI + \lambda A + \sum_j B_j(y) \frac{\partial}{\partial y_j} + C(y) \right) \phi = 0. \quad (109)$$

We label incoming and outgoing solutions by looking at $\Re\lambda$ for $\Re s$ sufficiently large. However, in the limit $\Re s \rightarrow 0$, we typically have $\Re\lambda \rightarrow 0$. The idea behind the layer construction is to modify the equation so that modes are damped as they propagate, meaning that $\Re\lambda$ is bounded away from zero for $\Re s \geq 0$. We also want to assure that there is no reflection at the interface between the physical and absorbing regions. The most direct way to do this is to design the problem in the layer so that its modal solutions for any s have the same eigenfunctions, ϕ , as (109).

Thus our starting point for constructing the layer is the formal modal solution:

$$\hat{u} = e^{\lambda x + (\lambda \hat{R}^{-1} - \mu) \int_0^x \sigma(z) dz} \phi. \quad (110)$$

In the examples we have carried through so far, R is a first order differential operator in time and the transverse variables with Laplace transform \hat{R} ,

$$R = \frac{\partial}{\partial t} + \sum_j \beta_j \frac{\partial}{\partial y_j} + \alpha, \quad (111)$$

μ is some number, and $\sigma \geq 0$ is the absorption parameter. We note that more complex choices for R and μ are certainly possible, for example R and μ could be defined by higher degree rational functions of s with operator or matrix coefficients. This may prove to be necessary to extend the method to other problems. We also note that if $\mu = 0$ and \hat{R} is represented by a function of s (and tangential wave numbers for constant coefficient problems), we can view the transformation as the result of extending x into the complex plane, as in [17] and its descendents.

It is now a simple matter to write down a system of equations satisfied by u in the layer. In particular, when we substitute (110) into the new system we want (109) to be the result. This yields:

$$\left(sI + (I - (R + \sigma)^{-1}\sigma)A \left(\frac{\partial}{\partial x} + \sigma\mu \right) + \sum_j B_j \frac{\partial}{\partial y_j} + C \right) \hat{u} = 0. \quad (112)$$

Introducing auxiliary functions w we finally obtain:

$$\frac{\partial u}{\partial t} + A(y) \left(\frac{\partial u}{\partial x} + \sigma\mu u \right) + \sum_j B_j(y) \frac{\partial u}{\partial y_j} + C(y)u + w = 0. \quad (113)$$

$$Rw + \sigma w + \sigma A(y) \left(\frac{\partial u}{\partial x} + \sigma\mu u \right) = 0. \quad (114)$$

We emphasize that the interface, $x = 0$, is nonreflecting for *any* choice of R , μ and σ . The difficulty is to choose them so that all waves are damped. Below we will examine some special constant coefficient cases where this can be achieved, albeit by inspection rather than by some systematic process.

A practical difficulty in implementing the PML is the choice of the absorption profile, σ . This is purely a numerical issue, as theoretically we can choose it to be constant and arbitrarily large. In our experiments we make it linear, and as our methods are high order we treat the interface as an internal boundary and use characteristic matching across it. However, we typically need to experiment to find near optimal slopes for the linear profile. The only serious analysis of this question which we are aware of is [19], where numerically optimal profiles for a specific discretization in the frequency domain are found.

Maxwell's Equations We return to (77)-(78), which we recall was the first system for which a PML was constructed [14]. Reordering the unknowns into the 6-vector $u = (E_x, B_x, E_y, B_y, E_z, B_z)^T$ we note that the matrix A is given in block form by:

$$A = c \begin{pmatrix} O & O & O \\ O & O & T \\ O & -T & 0 \end{pmatrix}, \quad T = \begin{pmatrix} 0 & 1 \\ -1 & 0 \end{pmatrix}. \quad (115)$$

From (114) and the structure of A we conclude that the first two components of w are zero. Thus we will take w to be a 4-vector appearing in the last four equations of (113) and (114). As the system has constant coefficients we may additionally perform a Fourier transformation in y and z . This leads to explicit expressions for λ :

$$\lambda = 0, \pm \left(\frac{s^2}{c^2} + k_x^2 + k_y^2 \right)^{1/2}, \quad (116)$$

which, of course, are by now quite familiar. Letting \bar{R} denote the symbol of R our problem is to guarantee:

$$\Re \left(\frac{\left(\frac{s^2}{c^2} + k_x^2 + k_y^2 \right)^{1/2}}{\bar{R}} - \mu \right) > 0. \quad (117)$$

A simple choice which by an easy calculation can be shown to satisfy (117) is:

$$R = \frac{s}{c} + \alpha, \quad \alpha \geq 0, \quad \mu = 0, \quad (118)$$

leading to the equations:

$$\frac{1}{c} \frac{\partial E}{\partial t} - \nabla \times B + \begin{pmatrix} 0 \\ w_y^{(E)} \\ w_z^{(E)} \end{pmatrix} = 0, \quad (119)$$

$$\frac{1}{c} \frac{\partial B}{\partial t} + \nabla \times E + \begin{pmatrix} 0 \\ w_y^{(B)} \\ w_z^{(B)} \end{pmatrix} = 0, \quad (120)$$

$$\left(\frac{1}{c} \frac{\partial}{\partial t} + \alpha + \sigma \right) w^{(E)} + \sigma \begin{pmatrix} \frac{\partial B_z}{\partial x} \\ -\frac{\partial B_y}{\partial x} \end{pmatrix} = 0, \quad (121)$$

$$\left(\frac{1}{c} \frac{\partial}{\partial t} + \alpha + \sigma \right) w^{(B)} + \sigma \begin{pmatrix} -\frac{\partial E_z}{\partial x} \\ \frac{\partial E_y}{\partial x} \end{pmatrix} = 0. \quad (122)$$

Although the equations themselves look quite different, a study of the eigenvalues reveals the formal equivalence between solutions of (119)-(122) and solutions in the layer constructed in [13]. In particular, the choice of $\alpha > 0$ corresponds to the complex frequency shift discussed in [13].

Linearized Euler Equations We now consider the linearized Euler equations, (83)-(85), again assuming a subsonic flow with $U_1 \neq 0$. Then A is nonsingular so that we require the full complement of auxiliary variables. Again we perform a Fourier-Laplace transformation and find that λ is given by:

$$\lambda = -\frac{\tilde{s}}{U_1}, \quad \frac{U_1 \tilde{s} \pm (\tilde{s}^2 + (1 - U_1^2)(k_y^2 + k_z^2))^{1/2}}{1 - U_1^2}, \quad (123)$$

$$\tilde{s} = s + ik_y U_2 + ik_z U_3. \quad (124)$$

We note the two distinct forms for λ , corresponding to the two types of waves.

We first choose \bar{R} in analogy with the case of Maxwell's equations,

$$\bar{R} = \tilde{s}, \quad (125)$$

is suggested. Then λ/\bar{R} is given by:

$$-\frac{1}{U_1}, \quad \frac{U_1}{1 - U_1^2} \pm \frac{(\tilde{s}^2 + (1 - U_1^2)(k_y^2 + k_z^2))^{1/2}}{(1 - U_1^2)\tilde{s}}. \quad (126)$$

Clearly when the square root is zero we can't have the correct sign on both terms. Thus we choose:

$$\mu = \frac{U_1}{1 - U_1^2}. \quad (127)$$

Now all terms now have the correct sign. We note that, as in (118), we could add a positive lower order term, α , to R . However, it would then be necessary to make μ dependent on \tilde{s} , leading to additional auxiliary variables.

We have carried out preliminary numerical experiments with the new layer for a problem defined by a periodic array of pressure pulses in the two-dimensional uniform flow $U_1 = 0.3$, $U_2 = 0.4$. The numerical method is eighth order in space and time. Relative errors as a function of time and average absorption parameter are listed in Table 3. Here the interior mesh is 258×64 while we have 34×64 points in each layer. The absorption profile is linear, and the layer is terminated by characteristic end conditions. Clearly, the accuracy is acceptable. Moreover, the insensitivity of the results to changes in $\bar{\sigma}$ indicates that the primary error source is the discretization itself. We note that the same problem has been solved in [48] using the Padé sequence of local boundary conditions, but there the solutions were better resolved so that the dominant error was due to the boundary condition. We plan to redo these computations so that direct comparisons can be made.

t	$\bar{\sigma} = 50$	$\bar{\sigma} = 75$	$\bar{\sigma} = 100$
1	1.6(-3)	1.6(-3)	1.6(-3)
2	1.4(-3)	1.4(-3)	1.4(-3)
4	1.1(-3)	1.1(-3)	1.1(-3)
8	1.3(-3)	1.4(-3)	1.4(-3)
16	2.4(-3)	2.5(-3)	2.9(-3)
32	3.4(-3)	2.4(-3)	2.4(-3)

Table 3. Relative errors - periodic array of pressure pulses, Euler PML $L = 1/2$

There have been other earlier attempts to generalize the PML to the Euler equations, beginning with Hu [68]. However, these all had stability problems [37, 58, 93]. Recent fixes in [2, 69] are restricted to flows aligned with the layer coordinate, while others [79] sacrifice the perfect matching property. Thus the general formulation developed here seems to have provided a convenient framework for constructing a true PML. We note that similar PMLs for advective problems have been constructed in [69, 11, 23].

Returning to the variable coefficient formulation, we have also begun experiments with the PML for linearizations about jet flow profiles [52]. A confounding factor in this case is the instability of the flow profile itself. Now the parameter μ is chosen numerically to suppress instabilities in the layer. So far, we have been unable to construct an absolutely stable layer, but we have been able to make the growth rate small enough that accurate results can be obtained over long time intervals.

Exterior Problems There are a variety of ways that the PML can be applied to problems in exterior domains. In particular, rectangles or convex regions of arbitrary aspect ratio can be used. This is, in our view, the primary advantage of the PML over high-order absorbing boundary conditions.

The standard approach is to use a rectangular box. Then, besides unidirectional layers attached to each face, there must be corner layers attached to the layers themselves. In these we use multiple sets of auxiliary variables. In a three dimensional corner, for example, we use three sets of auxiliary functions. Thus our general formulation would be:

$$\frac{\partial u}{\partial t} + \sum_j A_j \left(\frac{\partial}{\partial x_j} + \mu_j \right) u + Cu + \sum_j w^{(j)} = 0, \quad (128)$$

$$R_j w^{(j)} + \sigma_j A_j \left(\frac{\partial}{\partial x_j} + \mu_j \right) u + \sigma_j w^{(j)} = 0. \quad (129)$$

(Here we assume constant coefficients and rename the coefficient matrices.)

An alternative to a rectangular box is a curved boundary. Using the coordinate mapping technique, the PML has been extended to spheres and cylinders [94, 20, 82]. The idea is simply to apply the complex change of variables to the radial coordinate. For example, consider Maxwell's equations for a TE mode in two space dimensions using polar coordinates. Following [20] we make the change of variables:

$$r \rightarrow r \left(1 + \frac{c}{s} \bar{\sigma} \right), \quad \bar{\sigma} = r^{-1} \int_R^r \sigma(\rho) d\rho, \quad (130)$$

the equations for the Laplace transforms become:

$$\frac{s}{c} \hat{E}_r - \left(1 + \frac{c}{s} \bar{\sigma} \right)^{-1} \frac{1}{r} \frac{\partial \hat{B}_z}{\partial \theta} = 0, \quad (131)$$

$$\frac{s}{c}\hat{E}_\theta + \left(1 + \frac{c}{s}\sigma\right)^{-1} \frac{\partial \hat{B}_z}{\partial r} = 0, \quad (132)$$

$$\frac{s}{c}\hat{B}_z + \left(1 + \frac{c}{s}\sigma\right)^{-1} \frac{\partial \hat{E}_\theta}{\partial r} + \left(1 + \frac{c}{s}\bar{\sigma}\right)^{-1} \frac{1}{r}\hat{E}_\theta - \left(1 + \frac{c}{s}\bar{\sigma}\right)^{-1} \frac{1}{r} \frac{\partial \hat{E}_r}{\partial \theta} = 0. \quad (133)$$

Returning to the time domain we see that only a single auxiliary variable is needed:

$$\left(\frac{1}{c} \frac{\partial}{\partial t} + \bar{\sigma}\right) E_r - \frac{1}{r} \frac{\partial B_z}{\partial \theta} = 0, \quad (134)$$

$$\left(\frac{1}{c} \frac{\partial}{\partial t} + \sigma\right) E_\theta + \frac{\partial B_z}{\partial r} = 0, \quad (135)$$

$$\left(\frac{1}{c} \frac{\partial}{\partial t} + \bar{\sigma}\right) B_z + \frac{\partial E_\theta}{\partial r} + \frac{1}{r} E_\theta - \frac{1}{r} \frac{\partial E_r}{\partial \theta} + w = 0, \quad (136)$$

$$\left(\frac{1}{c} \frac{\partial}{\partial t} + \sigma\right) w + (\sigma - \bar{\sigma}) \frac{\partial E_\theta}{\partial r} = 0. \quad (137)$$

For scatterers which are well-fit by a sphere, this method has the advantage that it avoids the expensive corner regions where multiple sets of auxiliary functions are needed. Even more general curvilinear coordinates are considered in [96, 99]. Here the only restriction is that the local radii of curvature of the coordinate system remain positive.

Stability and Convergence To prove the convergence of the solutions obtained using the PML to the restriction to Ω of the unbounded domain solution one must establish the consistency of the method, as we have done in some cases for the boundary condition sequences, and its stability. In the frequency domain this has been carried out [74, 75, 66], but we know of no analogous results in the time domain. Stability, however, has been the focus of a great deal of analysis, which we will discuss below.

As first analyzed in [1], Bérenger's original formulation is not strongly well-posed, suggesting the possibility of instability and ill-posedness under perturbation. Later formulations, such as the ones presented in [82], are strongly well-posed. Strong well-posedness for (113)-(114) is easily analyzed. Freezing coefficients and performing a Fourier expansion in all spatial variables leads to the symbol of the PML equations:

$$\hat{P} = - \begin{pmatrix} ik_1 A + \sum_j ik_j B_j & O \\ \sigma ik_1 A & \sum_j ik_j \beta_j \end{pmatrix}. \quad (138)$$

Clearly, \hat{P} is diagonalizable assuming the strong hyperbolicity of the original problem whenever $\sum_j ik_j \beta_j$ is *not* an eigenvalue of $ik_1 A + \sum_j ik_j B_j$. If it is, the associated eigenvectors must be null vectors of A or we must have $k_1 = 0$. These conditions can be checked for our two examples.

Beyond strong well-posedness, which we see is independent of the sign of the damping term, σ , we require that the layer be asymptotically stable;

that is we require that no growing modes exist. This analysis is more difficult. However, for the Maxwell PML Bécache and Joly have recently developed an energy method which establishes this stronger form of stability [12, 13]. Interestingly the method does not apply when σ is variable, which is standard in practice. Therefore, the analysis of the asymptotic stability of the layer equations is an important open problem. One might hope that a new technique for treating this issue would lead to new insights into the construction of stable layers for variable coefficient problems.

3.2 Other Absorbing Layer Techniques

Although the PML has dominated the attention of the computational community in recent years, there are important problems to which it has not been applied. In many of these problems, older, ad hoc methods are still in use. A case of particular interest arises in the attempt to simulate the aeroacoustics of shear flows such as jets. Due to flow instabilities, both fine scale turbulence and large vortical structures are present at the outflow boundary. These certainly invalidate the analysis used to derive the PML and radiation boundary condition for the linearized Euler equations. Moreover, in practice the accuracy is also degraded, as shown in [21]. These authors suggest a different method, which seems to have become the method of choice at present for direct simulations of aeroacoustic phenomena [30, 76].

The basic description of the method of [21] is as follows; apply a smooth grid stretching in the absorbing region, which has the effect of making the propagating waves of shorter wavelength relative to the grid, and use some form of artificial viscosity or filtering to damp them. The computational experiments of [21] indicate that the method can be effective so long as the buffer zone is sufficiently wide.

In comparison with the PML, even more parameters need to be chosen without much theoretical guidance: grid stretching profiles, buffer zone lengths, and low-pass filters. As the method is clearly useful, we believe it would be of interest to develop some theory. An interesting move in this direction is the work in [22], which casts such procedures as a composition of grid mapping and filtering using the language of supergrid models. Although we emphasize that no hard error estimates directly follow, the formulation may be a good starting point.

3.3 PML for the Schrödinger Equation

Finally, we consider the construction of a PML for the Schrödinger equation. In [3, 77] they have been constructed using the complex coordinate stretching technique in more complicated settings than we will consider here, including systems describing excitons and one-way wave equations.

After Fourier-Laplace transformation, solutions of (97) are of exponential form with:

$$\lambda = \pm (-is + \kappa_j^2)^{1/2}. \quad (139)$$

As before, we seek to replace this in the layer by:

$$\lambda + \frac{\lambda}{\bar{R}} \int_0^x \sigma(z) dz. \quad (140)$$

We note that we must now also require continuity of $\frac{\partial u}{\partial x}$, so we will impose the additional condition:

$$\sigma(0) = 0. \quad (141)$$

Also, as the system is isotropic we don't require $\mu \neq 0$.

Unlike the exponents which we dealt with in the previous cases, the argument of λ now varies only between 0 and $-\frac{\pi}{2}$ when $\Re s > 0$. Thus it can be made to have a nonvanishing real part by a simple rotation. That is we can choose \bar{R} to be any complex number whose argument lies between 0 and $-\frac{\pi}{2}$. We thus obtain:

$$-i \frac{\partial u}{\partial t} = \frac{1}{1 + \sigma e^{i\gamma}} \frac{\partial}{\partial x} \left(\frac{1}{1 + \sigma e^{i\gamma}} \frac{\partial u}{\partial x} \right) + Lu, \quad 0 < \gamma < \frac{\pi}{2}. \quad (142)$$

Equation (142) has a clear interpretation. We simply make the system parabolic in the layer. However, note that increasing the absorption parameter σ corresponds to decreasing the diffusion coefficient, thus spawning a boundary layer at the interface. We also emphasize that, unlike the PML for hyperbolic equations, no additional variables are needed in the layer.

We have performed some simple one-dimensional numerical experiments with the Schrödinger PML. Choosing $\gamma = \frac{\pi}{4}$ we use second order differences and a second order BDF method in time. The layers contained twenty-five points, the absorption profile was quadratic, and the termination was with Dirichlet conditions. The solution, which we compute up to $T = 50$, was given initially by $(32/\pi)^{1/4} \exp(i\eta x - 16x^2)$, $\eta = 1, 10$. The errors as a function of $\bar{\sigma}$ and t are plotted in Figure 6. The results are quite good, though the reader should be cautioned that this is a one-dimensional experiment. They do show a difficult-to-predict dependence on $\bar{\sigma}$.

4 Conclusions and Open Problems

In summary, for a small but important list of problems domain truncation methods capable of delivering arbitrary accuracy at acceptable cost are now available to the computational scientist. These include the equations of acoustics, electromagnetics and elastodynamics in homogeneous media and waveguide or exterior geometries. Certainly there is room for improvement in the efficiency and the mathematical analysis of these successful methods, but we believe they are already well-grounded, reliable tools.

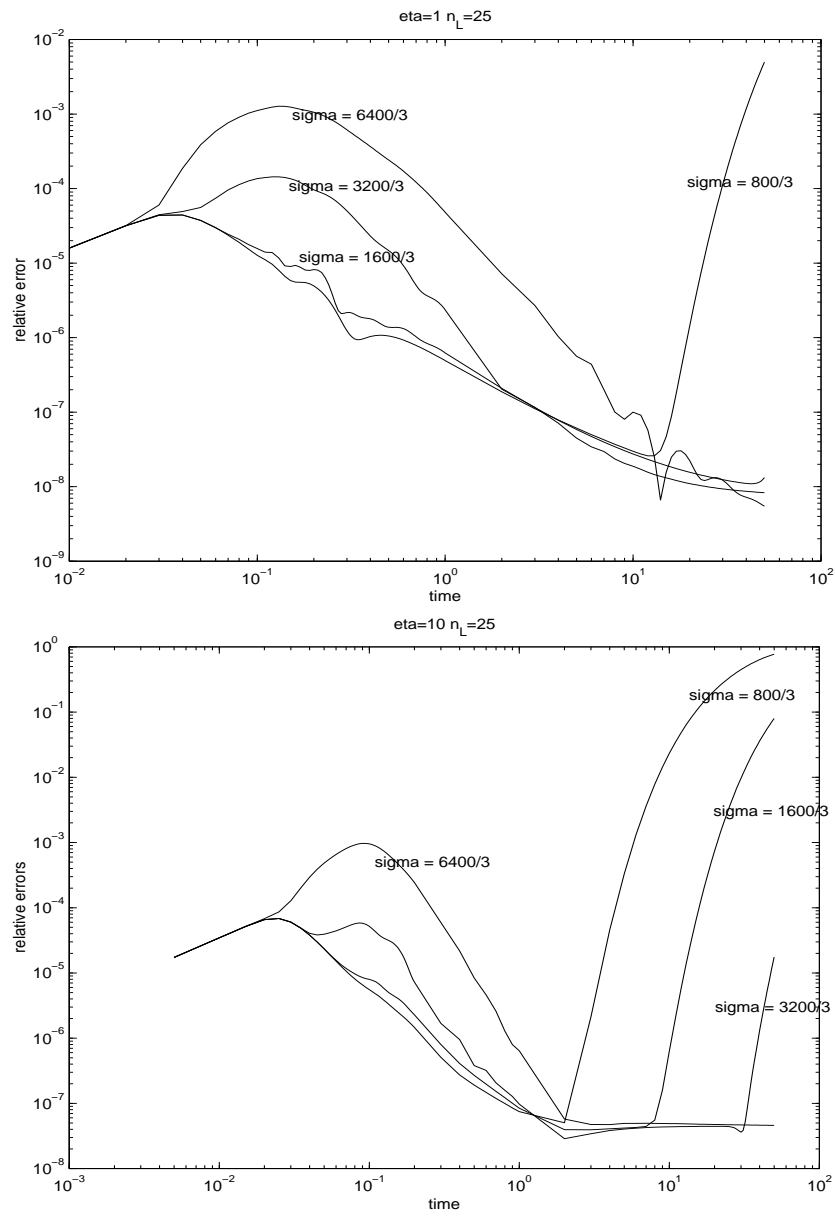


Fig. 6. Errors for the Schrodinger PML, 25-point layer, $\eta = 1, 10$.

As we've presented a number of different techniques, it is natural to try to compare them. At present, it would be premature to definitively claim that one or the other is best. For a fixed domain configuration, it is the author's experience that high-order boundary condition methods are somewhat more efficient and easy to use than the PML. This is due to the fact that the PML depends on the choice of the absorption profile and on adding points in a volume distribution to achieve convergence, whereas the boundary condition methods only require the addition of auxiliary functions. On the other hand, the PML can be used in arbitrary convex domains, and thus is currently more efficient for high-aspect ratio scatterers. Comparing boundary conditions, the nonlocal approximations are the clear winners from the point of view of complexity analysis. However, the local sequences are easier to implement, and often require many fewer auxiliary functions than the error analyses suggest. Thus they can be competitive if a good adaptive strategy can be found.

We have identified a number of important open problems whose resolution is likely to have the final say on the future importance of the various accurate techniques. These include:

- i. Extension of the high-order local and/or nonlocal boundary conditions to high-aspect ratio boundaries such as boxes or spheroids.
- ii. Sharp error analysis for the time-domain PML, particularly in high-aspect ratio domains.
- iii. Convergence analysis of Higdon-type boundary conditions for problems with variable coefficients.
- iv. Improved understanding of the stability of PMLs leading to their extension to a wider range of problems including those with variable coefficients.
- v. Adaptive order determination for local boundary condition sequences.
- vi. Optimization of absorption parameters in the PML.
- vii. Mathematical analysis of alternative absorbing layer methods.

We believe that progress on these issues is possible, and that it will lead to substantial improvements in our ability to simulate waves.

References

1. S. Abarbanel and D. Gottlieb. A mathematical analysis of the PML method. *J. Comput. Phys.*, 134:357–363, 1997.
2. S. Abarbanel, D. Gottlieb, and J. Hesthaven. Well-posed perfectly matched layers for advective acoustics. *J. Comput. Phys.*, 154:266–283, 1999.
3. A. Ahland, D. Schulz, and E. Voges. Accurate mesh truncation for Schrödinger equations by a perfectly matched layer absorber: Application to the calculation of optical spectra. *Phys. Rev. B*, 60:5109–5112, 1999.

4. I. Alonso-Mallo and N. Reguera. Weak ill-posedness of spatial discretizations of absorbing boundary conditions for Schrödinger-type equations. *SIAM J. Numer. Anal.*, 40:134–158, 2002.
5. B. Alpert, L. Greengard, and T. Hagstrom. Rapid evaluation of nonreflecting boundary kernels for time-domain wave propagation. *SIAM J. Numer. Anal.*, 37:1138–1164, 2000.
6. B. Alpert, L. Greengard, and T. Hagstrom. Nonreflecting boundary conditions for the time-dependent wave equation. *J. Comput. Phys.*, 180:270–296, 2002.
7. X. Antoine and H. Barucq. Microlocal diagonalization of strictly hyperbolic pseudodifferential systems and application to the design of radiation boundary conditions in electromagnetism. *SIAM J. Appl. Math.*, 61:1877–1905, 2001.
8. R.J. Astley. Transient spheroidal elements for unbounded wave problems. *Computer Meth. Appl. Mech. Engrg.*, 164:3–15, 1998.
9. R.J. Astley. Infinite elements for wave problems: A review of current formulations and an assessment of accuracy. *Int. J. for Numer. Meth. Engrg.*, 49:951–976, 2000.
10. R.J. Astley and J. Hamilton. Infinite elements for transient flow acoustics. Technical Report 2001-2273, AIAA, 2002.
11. E. Bécache, A.-S. Bonnet-Ben Dhia, and G. Legendre. Perfectly matched layers for the convected Helmholtz equation. In preparation, 2002.
12. E. Bécache and P. Joly. On the analysis of Bérenger's perfectly matched layers for Maxwell's equations. *Math. Model. and Numer. Anal.*, 36:87–119, 2002.
13. E. Bécache, P. Petropoulos, and S. Gedney. On the long-time behavior of unsplit Perfectly Matched Layers. Preprint, 2002.
14. J.-P. Bérenger. A perfectly matched layer for the absorption of electromagnetic waves. *J. Comput. Phys.*, 114:185–200, 1994.
15. A. Barry, J. Bielak, and R.C. MacCamy. On absorbing boundary conditions for wave propagation. *J. Comput. Phys.*, 79:449–468, 1988.
16. A. Bayliss and E. Turkel. Radiation boundary conditions for wave-like equations. *Comm. Pure and Appl. Math.*, 33:707–725, 1980.
17. W. Chew and W. Weedon. A 3-D perfectly matched medium from modified Maxwell's equations with stretched coordinates. *Microwave Optical Technol. Lett.*, 7:599–604, 1994.
18. F. Collino. High order absorbing boundary conditions for wave propagation models. Straight line boundary and corner cases. In R. Kleinman et al., editor, *Proceedings of 2nd Int. Conf. on Math. and Numer. Aspects of Wave Prop. Phen.*, pages 161–171. SIAM, 1993.
19. F. Collino and P. Monk. Optimizing the perfectly matched layer. *Computer Meth. Appl. Mech. Engrg.*, 164:157–171, 1998.
20. F. Collino and P. Monk. The perfectly matched layer in curvilinear coordinates. *SIAM J. Sci. Comput.*, 19:2061–2090, 1998.
21. T. Colonius, S. Lele, and P. Moin. Boundary conditions for direct computation of aerodynamic sound generation. *AIAA J.*, 31:1574–1582, 1993.
22. T. Colonius and H. Ran. A super-grid scale model for simulating compressible flow on unbounded domains. *J. Comput. Phys.*, 2002. To appear.
23. J. Diaz and P. Joly. Stabilized perfectly matched layers for advective wave equations. In preparation, 2002.
24. L. DiMenza. Transparent and absorbing boundary conditions for the Schrödinger equation in a bounded domain. *Numer. Funct. Anal. Optim.*, 18:759–775, 1997.

25. B. Engquist and L. Halpern. Far field boundary conditions for computation over long time. *Appl. Numer. Math.*, 4:21–45, 1988.
26. B. Engquist and A. Majda. Absorbing boundary conditions for the numerical simulation of waves. *Math. Comp.*, 31:629–651, 1977.
27. B. Engquist and A. Majda. Radiation boundary conditions for acoustic and elastic wave calculations. *Comm. Pure and Appl. Math.*, 32:313–357, 1979.
28. A. Ergin, B. Shanker, and E. Michielssen. Fast evaluation of three-dimensional transient wave fields using diagonal translation operators. *J. Comput. Phys.*, 146:157–180, 1998.
29. T. Fevens and H. Jiang. Absorbing boundary conditions for the Schrödinger equation. *SIAM J. Sci. Comput.*, 21:255–282, 1999.
30. J. Freund and S. Lele. Computer simulation and prediction of jet noise. In *High Speed Jet Flows: Fundamentals and Applications*. Taylor Francis, 2001.
31. T. Geers. Singly and doubly asymptotic computational boundaries. In *Computational Methods for Unbounded Domains*, pages 135–142, Dordrecht, the Netherlands, 1998. Kluwer Academic Publishers.
32. M. Giles. Nonreflecting boundary conditions for Euler equation calculations. *AIAA Journal*, 28:2050–2058, 1990.
33. D. Givoli. Exact representations on artificial interfaces and applications in mechanics. *Appl. Mech. Rev.*, 52:333–349, 1999.
34. D. Givoli and D. Kohen. Non-reflecting boundary conditions based on Kirchoff-type formulae. *J. Comput. Phys.*, 117:102–113, 1995.
35. D. Givoli and B. Neta. High-order nonreflecting boundary scheme for time-dependent waves. *J. Comput. Phys.*, 2002. To appear.
36. D. Givoli, B. Neta, and I. Patlashenko. Finite element solution of exterior time-dependent wave problems with high-order boundary treatment. Submitted, 2002.
37. J. Goodrich and T. Hagstrom. A comparison of two accurate boundary treatments for computational aeroacoustics. In *3rd AIAA/CEAS Aeroacoustics Conference*, 1997.
38. L. Greengard and V. Rokhlin. A new version of the fast multipole method for the Laplace equation in three dimensions. *Acta Numerica*, 6:229–269, 1997.
39. M. Grote. Nonreflecting boundary conditions for elastodynamic scattering. *J. Comput. Phys.*, 161:331–353, 2000.
40. M. Grote and J. Keller. Exact nonreflecting boundary conditions for the time dependent wave equation. *SIAM J. Appl. Math.*, 55:280–297, 1995.
41. M. Grote and J. Keller. Nonreflecting boundary conditions for time dependent scattering. *J. Comput. Phys.*, 127:52–81, 1996.
42. M. Grote and J. Keller. Nonreflecting boundary conditions for Maxwell's equations. *J. Comput. Phys.*, 139:327–342, 1998.
43. M. Grote and J. Keller. Exact nonreflecting boundary conditions for elastic waves. *SIAM J. Appl. Math.*, 60:803–818, 2000.
44. M. Guddati and J. Tassoulas. Continued-fraction absorbing boundary conditions for the wave equation. *J. Comput. Acoust.*, 8:139–156, 1998.
45. T. Hagstrom. On the convergence of local approximations to pseudodifferential operators with applications. In E. Bécache, G. Cohen, P. Joly, and J. Roberts, editors, *Proc. of the 3rd Int. Conf. on Math. and Numer. Aspects of Wave Prop. Phen.*, pages 474–482. SIAM, 1995.

46. T. Hagstrom. On high-order radiation boundary conditions. In B. Engquist and G. Kriegsmann, editors, *IMA Volume on Computational Wave Propagation*, pages 1–22, New York, 1996. Springer-Verlag.
47. T. Hagstrom. Radiation boundary conditions for the numerical simulation of waves. *Acta Numerica*, 8:47–106, 1999.
48. T. Hagstrom and J. Goodrich. Accurate radiation boundary conditions for the linearized Euler equations in Cartesian domains. *SIAM J. Sci. Comput.*, 2002. To appear.
49. T. Hagstrom and S.I. Hariharan. A formulation of asymptotic and exact boundary conditions using local operators. *Appl. Numer. Math.*, 27:403–416, 1998.
50. T. Hagstrom, S.I. Hariharan, and R. MacCamy. On the accurate long-time solution of the wave equation on exterior domains: Asymptotic expansions and corrected boundary conditions. *Math. Comp.*, 63:507–539, 1994.
51. T. Hagstrom, S.I. Hariharan, and D. Thompson. High-order radiation boundary conditions the convective wave equation in exterior domains. Submitted.
52. T. Hagstrom and I. Nazarov. Absorbing layers and radiation boundary conditions for jet flow simulations. Technical Report AIAA 2002-2606, AIAA, 2002.
53. T. Hagstrom and T. Warburton. High-order radiation boundary conditions for time-domain electromagnetics using unstructured discontinuous Galerkin methods. In preparation, 2002.
54. E. Hairer, C. Lubich, and M. Schlichte. Fast numerical solution of nonlinear Volterra convolutional equations. *SIAM J. Sci. Stat. Comput.*, 6:532–541, 1985.
55. L. Halpern and J. Rauch. Error analysis for absorbing boundary conditions. *Numer. Math.*, 51:459–467, 1987.
56. L. Halpern and L. Trefethen. Wide-angle one-way wave equations. *J. Acoust. Soc. Am.*, 84:1397–1404, 1988.
57. D. Healy, D. Rockmore, P. Kostelec, and S. Moore. FFTs for the 2-sphere - Improvements and variations. *Adv. Appl. Math.*, 2002. To appear.
58. J. Hesthaven. On the analysis and construction of perfectly matched layers for the linearized Euler equations. *J. Comput. Phys.*, 142:129–147, 1998.
59. J. Hesthaven and T. Warburton. High-order/spectral methods on unstructured grids. I. Time-domain solution of Maxwell's equations. *J. Comput. Phys.*, 181:186–221, 2002.
60. R. Higdon. Absorbing boundary conditions for difference approximations to the multidimensional wave equation. *Math. Comp.*, 47:437–459, 1986.
61. R. Higdon. Numerical absorbing boundary conditions for the wave equation. *Math. Comp.*, 49:65–90, 1987.
62. R. Higdon. Radiation boundary conditions for elastic wave propagation. *SIAM J. Numer. Anal.*, 27:831–870, 1990.
63. R. Higdon. Absorbing boundary conditions for elastic waves. *Geophysics*, 56:231–254, 1991.
64. R. Higdon. Absorbing boundary conditions for acoustic and elastic waves in stratified media. *J. Comput. Phys.*, 101:386–418, 1992.
65. R. Higdon. Radiation boundary conditions for dispersive waves. *SIAM J. Numer. Anal.*, 31:64–100, 1994.

66. T. Hohage, F. Schmidt, and L. Zschiedrich. Solving time-harmonic scattering problems based on the pole condition: Convergence of the PML method. Technical Report ZIB-Report 01-23, Zuse Institut Berlin, 2001.
67. R. Holford. A multipole expansion for the acoustic field exterior to a prolate or oblate spheroid. Preprint, 1998.
68. F. Hu. On absorbing boundary conditions for linearized Euler equations by a perfectly matched layer. *J. Comput. Phys.*, 129:201–219, 1996.
69. F. Hu. A stable, perfectly matched layer for linearized Euler equations in unsplit physical variables. *J. Comput. Phys.*, 173:455–480, 2001.
70. R. Huan and L. Thompson. Accurate radiation boundary conditions for the time-dependent wave equation on unbounded domains. *Int. J. Numer. Meth. Engrg.*, 47:1569–1603, 2000.
71. M. Israeli and S. Orszag. Approximation of radiation boundary conditions. *J. Comput. Phys.*, 41:115–135, 1981.
72. S. Jiang. *Fast Evaluation of Nonreflecting Boundary Conditions for the Schrödinger Equation*. PhD thesis, New York University, 2001.
73. H.-O. Kreiss and J. Lorenz. *Initial-Boundary Value Problems and the Navier-Stokes Equations*. Academic Press, New York, 1989.
74. M. Lassas and E. Somersalo. On the existence and convergence of the solution of PML equations. *Computing*, 60:228–241, 1998.
75. M. Lassas and E. Somersalo. Analysis of the PML equations in general convex geometry. *Proc. Roy. Soc. Edinburgh A*, 131:1183–1207, 2001.
76. S. Lele. Direct numerical simulation of compressible turbulent flows: fundamentals and applications. In A. Hanifi, P. Alfredsson, A. Johansson, and D. Henningson, editors, *Transition, Turbulence and Combustion Modelling*, chapter 7. Kluwer, Dordrecht, 1999.
77. M. Levy. Perfectly matched layer truncation for parabolic wave equation models. *Proc. Roy. Soc. Lond. A*, 457:2609–2624, 2001.
78. E. Lindman. Free space boundary conditions for the time dependent wave equation. *J. Comput. Phys.*, 18:66–78, 1975.
79. J.-L. Lions, J. Métral, and O. Vacus. Well-posed absorbing layer for hyperbolic problems. *Numer. Math.*, 2001. To appear.
80. C. Lubich and A. Schädle. Fast convolution for non-reflecting boundary conditions. *SIAM J. Sci. Comput.*, 24:161–182, 2002.
81. M. Mohlenkamp. A fast transform for spherical harmonics. *J. of Fourier Anal. and Applic.*, 5:159–184, 1999.
82. P. Petropoulos. Reflectionless sponge layers as absorbing boundary conditions for the numerical solution of Maxwell's equations in rectangular, cylindrical and spherical coordinates. *SIAM J. Appl. Math.*, 60:1037–1058, 2000.
83. C. Randall. Absorbing boundary condition for the elastic wave equation. *Geophysics*, 53:611–624, 1988.
84. C. Rowley and T. Colonius. Discretely nonreflecting boundary conditions for linear hyperbolic systems. *J. Comput. Phys.*, 15:500–538, 2000.
85. V. Ryabe'nkii. *Method of Difference Potentials and its Applications*. Springer-Verlag, New York, 2001.
86. V. Ryaben'kii, S. Tsynkov, and V. Turchaninov. Global discrete artificial boundary conditions for time-dependent wave propagation. *J. Comput. Phys.*, 174:712–758, 2001.

87. V. Ryaben'kii, S. Tsynkov, and V. Turchaninov. Long-time numerical computation of wave-type solutions driven by moving sources. *Appl. Numer. Math.*, 38:187–222, 2001.
88. A. Schädle. *Ein Schneller Faltungsalgorithmus für Nichtreflektierende Randbedingungen*. PhD thesis, Eberhard-Karls-Universität Tübingen, 2002.
89. I. Sofronov. Conditions for complete transparency on the sphere for the three-dimensional wave equation. *Russian Acad. Sci. Dokl. Math.*, 46:397–401, 1993.
90. I. Sofronov. Artificial boundary conditions of absolute transparency for two- and three-dimensional external time-dependent scattering problems. *Euro. J. Appl. Math.*, 9:561–588, 1998.
91. I. Sofronov. Non-reflecting inflow and outflow in wind tunnel for transonic time-accurate simulation. *J. Math. Anal. Appl.*, 221:92–115, 1998.
92. R. Suda and M. Takami. A fast spherical harmonic transform algorithm. *Math. Comput.*, 71:703–715, 2002.
93. C. Tam, L. Auriault, and F. Cambuli. Perfectly matched layer as an absorbing boundary condition for the linearized Euler equations in open and ducted domains. *J. Comput. Phys.*, 144:213–234, 1998.
94. F. Teixeira and W. Chew. PML-FDTD in cylindrical and spherical grids. *IEEE Microwave and Guided Wave Lett.*, 7:285–287, 1997.
95. F. Teixeira and W. Chew. Systematic derivation of anisotropic PML absorbing media in cylindrical and spherical coordinates. *IEEE Microwave and Guided Wave Lett.*, 7:371–373, 1997.
96. F. Teixeira and W. Chew. Analytical derivation of a conformal perfectly matched absorber for electromagnetic waves. *Microwave and Optical Tech. Lett.*, 17:231–236, 1998.
97. F. Teixeira and W. Chew. General closed-form PML constitutive tensors to match arbitrary bianisotropic and dispersive linear media. *IEEE Microwave and Guided Wave Lett.*, 8:223–225, 1998.
98. F. Teixeira and W. Chew. Finite-difference computation of transient electromagnetic waves for cylindrical geometries in complex media. *IEEE Trans. on Geosci. and Remote Sensing*, 38:1530–1543, 2000.
99. F. Teixeira, K.-P. Hwang, W. Chew, and J.-M. Jin. Conformal PML-FDTD schemes for electromagnetic field simulations: A dynamic stability study. *IEEE Trans. on Ant. Prop.*, 49:902–907, 2001.
100. L. Thompson and R. Huan. Implementation of exact non-reflecting boundary conditions in the finite element method for the time-dependent wave equation. *Comput. Methods Appl. Mech. Engrg.*, 187:137–159, 2000.
101. L. Ting and M. Miksis. Exact boundary conditions for scattering problems. *J. Acoust. Soc. Am.*, 80:1825–1827, 1986.
102. O. Vacus. Mathematical analysis of absorbing boundary conditions for the wave equation: The corner problem. *Math. Comput.*, 2002. To appear.
103. H. Warchall. Wave propagation at computational domain boundaries. *Commun. in Part. Diff. Eq.*, 16:31–41, 1991.
104. L. Xu. *Applications of High-Order Radiation Boundary Conditions*. PhD thesis, The University of New Mexico, 2001.
105. C. Zhao and T. Liu. Non-reflecting artificial boundaries for modelling scalar wave propagation problems in two-dimensional half space. *Comput. Meth. Appl. Mech. Engrg.*, 191:4569–4585, 2002.